Annual Review of Earth and Planetary Sciences

Carbon Fluxes in the Coastal Ocean: Synthesis, Boundary Processes and Future Trends

Minhan Dai,[1] Jianzhong Su,[1] Yangyang Zhao,[1] Eileen E. Hofmann,[2] Zhimian Cao,[1] Wei-Jun Cai,[3] Jianping Gan,[4] Fabrice Lacroix,[5] Goulven G. Laruelle,[6] Feifei Meng,[1] Jens Daniel Müller,[7] Pierre A.G. Regnier,[6] Guizhi Wang,[1] and Zhixuan Wang[1]

[1]State Key Laboratory of Marine Environmental Science & College of Ocean and Earth Sciences, Xiamen University, Xiamen, China; email: mdai@xmu.edu.cn

[2]Center for Coastal Physical Oceanography, Old Dominion University, Norfolk, Virginia, USA

[3]School of Marine Science and Policy, University of Delaware, Newark, Delaware, USA

[4]Departments of Ocean Science and Mathematics, The Hong Kong University of Science and Technology, Kowloon, Hong Kong SAR, China

[5]Department of Biogeochemical Signals, Max Planck Institute for Biogeochemistry, Jena, Germany

[6]Biogeochemistry and Modelling of the Earth System (BGEOSYS), Department of Geoscience, Environment & Society, Université Libre de Bruxelles, Brussels, Belgium

[7]Department of Environmental Systems Science, Institute of Biogeochemistry and Pollutant Dynamics, ETH Zurich, Zurich, Switzerland

Annu. Rev. Earth Planet. Sci. 2022. 50:593–626

The *Annual Review of Earth and Planetary Sciences* is online at earth.annualreviews.org

https://doi.org/10.1146/annurev-earth-032320-090746

Keywords

carbon cycle, coastal ocean, air-sea CO_2 flux, continental margin, river-dominated ocean margin, RiOMar, ocean-dominated margin, OceMar, carbon neutrality

Abstract

This review examines the current understanding of the global coastal ocean carbon cycle and provides a new quantitative synthesis of air-sea CO_2 exchange. This reanalysis yields an estimate for the globally integrated coastal ocean CO_2 flux of -0.25 ± 0.05 Pg C year^{-1}, with polar and subpolar regions accounting for most of the CO_2 removal (>90%). A framework that classifies river-dominated ocean margin (RiOMar) and ocean-dominated margin (OceMar) systems is used to conceptualize

coastal carbon cycle processes. The carbon dynamics in three contrasting case study regions, the Baltic Sea, the Mid-Atlantic Bight, and the South China Sea, are compared in terms of the spatio-temporal variability of surface pCO_2. Ocean carbon models that range from box models to three-dimensional coupled circulation-biogeochemical models are reviewed in terms of the ability to simulate key processes and project future changes in different continental shelf regions. Common unresolved challenges remain for implementation of these models across RiOMar and OceMar systems. The long-term trends in coastal ocean carbon fluxes for different coastal systems under anthropogenic stress that are emerging in observations and numerical simulations are highlighted. Knowledge gaps in projecting future perturbations associated with before and after net-zero CO_2 emissions in the context of concurrent changes in the land-ocean-atmosphere coupled system pose a key challenge.

- A new synthesis yields an estimate for globally integrated coastal ocean carbon sink of -0.25 Pg C year^{-1}, with greater than 90% of atmospheric CO_2 removal occurring in polar and subpolar regions.
- The sustained coastal and open ocean carbon sink is vital in mitigating climate change and meeting the target set by the Paris Agreement.
- Uncertainties in the future coastal ocean carbon cycle are associated with concurrent trends and changes in the land-ocean-atmosphere coupled system.
- The major gaps and challenges identified for current coastal ocean carbon research have important implications for climate and sustainability policies.

1. INTRODUCTION

Ocean sequestration of atmospheric CO_2 is increasingly recognized as an important climate mitigation pathway to realize the target of a 1.5–2.0°C temperature increase set by the Paris Agreement (Aricò et al. 2021, Pörtner et al. 2019) (see Sidebar titled Key Terms). The sustained ocean carbon sink is vital in meeting this target because it accounts for an overall uptake of ∼37% of the fossil fuel CO_2 emissions, or ∼25% of the combined fossil fuel burning and emissions due to land use changes between 1850 and 2019 (Friedlingstein et al. 2020). Hoegh-Guldberg et al. (2019) further projected that ocean-based mitigation options could reduce the emissions gap by up to ∼21% for a 1.5°C pathway and by ∼25% for a 2.0°C pathway, making the ocean a primary carbon sink.

Though relatively small in surface area, the coastal ocean (defined in this review as ocean margin or continental margin as detailed in **Supplemental Material Section 1**), with its rich spatial, economic, and biological resources and diverse ecosystems, provides important ecosystem services in support of human society. The absorption of anthropogenic CO_2 is one of the most important ecosystem services provided by the coastal ocean and its associated nearshore ecosystems (e.g., Cooley et al. 2009).

The coastal ocean is characterized by elevated primary production and is the site for long-term burial of organic matter and calcium carbonate ($CaCO_3$), both important contributors to the global carbon budget (Gattuso et al. 1998, Mackenzie et al. 2005). The coastal ocean provides a highly dynamic land-ocean interface where biogeochemical processes modulate and transform carbon inputs from both land and the open ocean, thereby controlling subsequent air-sea CO_2 exchanges and exports of carbon to the open ocean (Bauer et al. 2013, Cai 2011, Chen & Borges 2009, Hofmann et al. 2011, Lacroix et al. 2021a). This role of the coastal ocean makes its inclusion as a component of the global carbon cycle critical for development of carbon and climate policies. The complexity of processes in the coastal ocean, however, presents significant challenges for

KEY TERMS

Acronyms, Abbreviations, and Symbols

CO_2: carbon dioxide
DIC: dissolved inorganic carbon
TA: total alkalinity
pCO_2: partial pressure of CO_2
HCO_3^- : bicarbonate
$CaCO_3$: calcium carbonate
NO_3: nitrate
NO_2: nitrite
PO_4: phosphate
SST: sea surface temperature
MARCATS: MARgins and CATchment Segmentation
SD: Standard Deviation
NEP: net ecosystem production
NEC: net ecosystem calcification
CDR: carbon dioxide removal
ESMs: Earth system models
GOBMs: global ocean biogeochemical models
OceMar: ocean-dominated margin
RiOMar: river-dominated ocean margin
EBC: eastern boundary current
WBC: western boundary current
SCS: South China Sea
WNP: western North Pacific
BS: Baltic Sea
MAB: Mid-Atlantic Bight
ECS: East China Sea
SEATS: Southeastern Asia Time-series Study
RCP: representative concentration pathway
SOCAT: Surface Ocean CO_2 Atlas

Variables

R_{CO2}: the air-sea CO_2 flux
F_{DIC}: the input or output flux of DIC across the boundary
$\partial DIC/\partial t$: the change in the amount of DIC over time
$NO_3 + NO_2$: the sum of concentrations of nitrate and nitrite
PO_4: the phosphate concentration
δDIC^*: changes in the DIC concentration solely induced by air-sea CO_2 exchange
ΔpCO_2: the difference in the partial pressure of CO_2 (pCO_2) between seawater and the atmosphere

its inclusion in Earth system models, one of the essential tools for developing climate and sustainability policies.

Sink of atmospheric CO_2: uptake of CO_2 from the atmosphere by the ocean

The removal (uptake) or release of CO_2 from or to the atmosphere is referred as a sink or source of atmospheric CO_2, respectively (**Figure 1*a***). By convention, the ocean's uptake of CO_2 from the

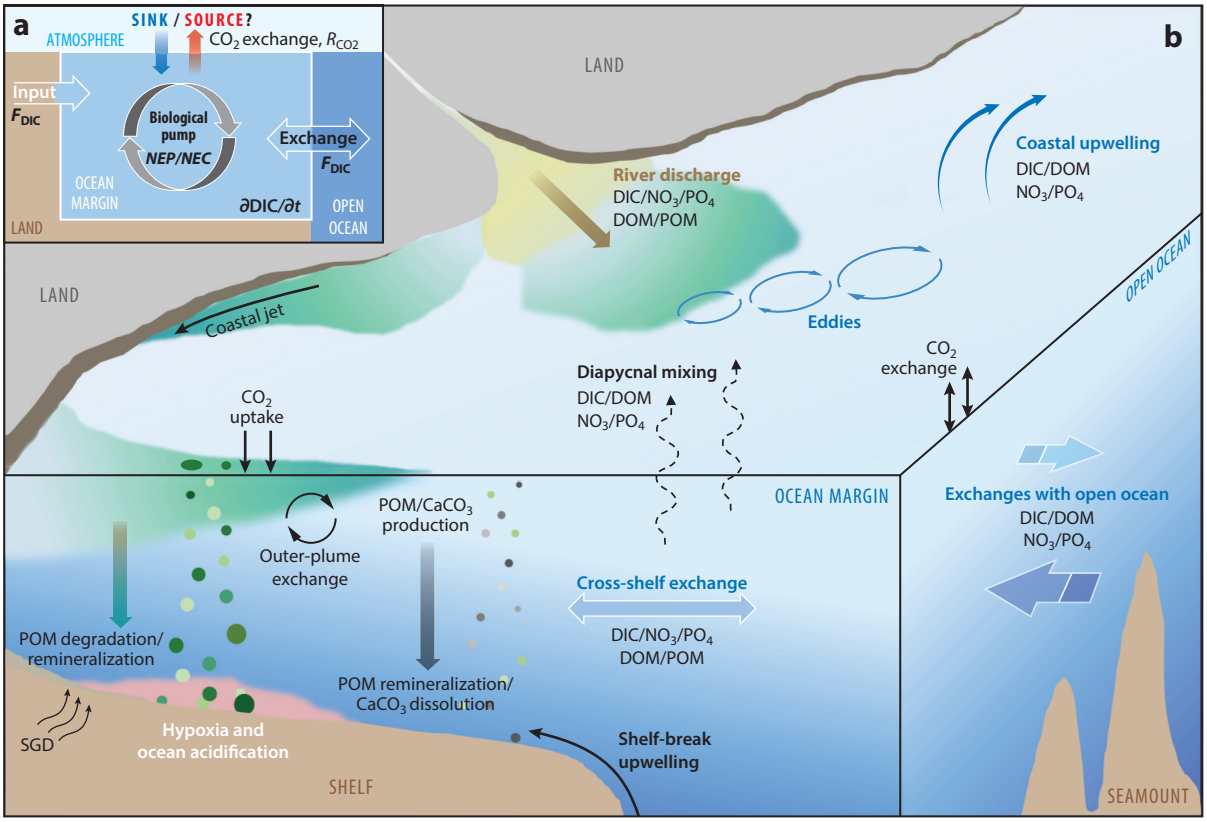

Figure 1

Conceptual schematics of air-sea CO_2 exchanges (*a*) and major physical and biogeochemical processes in the coastal ocean (*b*), highlighting the transport of matter between land, ocean margin, and open ocean. (*a*) The sea-air CO_2 flux (R_{CO2}) is balanced by the sum of DIC inputs and outputs (F_{DIC}) across the boundaries, the NEP and NEC, and the change in the amount of DIC over time ($\partial DIC/\partial t$) within the coastal system (Equation 1 in the text). (*b*) The ocean margin is bordered by the coastline on the land side and by the open ocean on the outer side. Rivers discharge DIC, NO_3, PO_4, DOM, and POM onto the continental shelf via a buoyant plume, and SGD also provides important fluxes of carbon and nutrients to coastal waters. The riverine nutrients stimulate enhanced phytoplankton growth and POM production in the mid- and far fields of the plume, which exchanges with oceanic waters at plume fronts and can extend beyond the shelf break when entrained by sub-meso- and mesoscale eddies. The POM that is produced sinks and is degraded or remineralized in bottom waters, leading to severe consequences such as hypoxia and OA. Wind-induced upwelling at the shelf break and in nearshore regions, and upward diapycnal mixing also supply nutrients as well as DIC and DOM to the surface, facilitating primary production (POM/$CaCO_3$ production). The POM is remineralized and $CaCO_3$ is dissolved when sinking to deep waters. The biogeochemistry of upwelled or upward mixed waters is controlled by the exchange of DIC, nutrients, DOM, and/or POM at the ocean margin-open ocean interface. The sea-air CO_2 exchange ultimately depends on the relative supply or consumption of DIC and nutrients due to water mass mixing and the intrinsic biological metabolism. Panel *b* is adapted from Liu et al. (2010). Abbreviations: $CaCO_3$, calcium carbonate; DIC, dissolved inorganic carbon; DOM, dissolved organic matter; NEC, net ecosystem calcification; NEP, net ecosystem production; NO_3, nitrate; OA, ocean acidification; PO_4, phosphate; POM, particulate organic matter; SGD, submarine ground discharge.

Source of atmospheric CO_2: transfer of CO_2 out of the ocean to the atmosphere

atmosphere (sink) is indicated by a negative sign, and release of CO_2 into the atmosphere (source) is indicated by a positive sign. The role of the coastal ocean as a source or sink of atmospheric CO_2 in the global carbon budget has received considerable attention (e.g., Borges et al. 2005, Cai & Dai 2004, Cai et al. 2006, Chen & Borges 2009, Dai et al. 2013, Laruelle et al. 2014, Roobaert et al. 2019, Thomas et al. 2004). The current role of the global ocean margin as a carbon sink is

relatively well constrained, ranging from −0.19 to −0.45 Pg C year^{-1} with a flux density between −0.5 and −1.0 mol C m^{-2} year^{-1} (Borges et al. 2005, Cai et al. 2006, Chen et al. 2013, Dai et al. 2013, Laruelle et al. 2014), with more recent estimates pointing toward the lower bound of these ranges (Roobaert et al. 2019). However, these global flux estimates are only beginning to resolve the seasonality and heterogeneity of regional ocean margin systems (Roobaert et al. 2019), many of which are known to alternate between carbon sinks and sources at different spatial and temporal scales (e.g., Cai et al. 2020). The basic spatial patterns of CO_2 fluxes provided by regional observational programs show that individual coastal ocean regions have extensive spatial variability, making it difficult to categorize coastal ocean systems and quantify these fluxes (e.g., Cai et al. 2020, Guo et al. 2015, Li et al. 2020b). Temporal variability of the coastal ocean CO_2 flux is even less well known, although understanding of its seasonality is emerging (e.g., Guo et al. 2015). Finally, interannual variability or long-term temporal trends of coastal ocean CO_2 fluxes remain elusive and controversial (e.g., Laruelle et al. 2018).

A simplified mass balance equation (Cao et al. 2020, Mackenzie & Lerman 2006) provides a framework to examine the processes and mechanisms that control the air-sea CO_2 flux (R_{CO2}, **Figure 1*a***) as:

$$R_{CO2} = \sum F_{DIC} + NEP + NEC + \partial DIC/\partial t, \quad 1.$$

where $\sum F_{DIC}$ is the sum of the dissolved inorganic carbon (DIC) inputs and outputs, *NEP* and *NEC* are the net ecosystem production and calcification, respectively, and $\partial DIC/\partial t$ is the change in the amount of DIC over time, which is assumed to be zero at steady state ($\partial DIC/\partial t \sim 0$). In most coastal regions, NEC is relatively small except for some tropical continental shelves with coral reefs and carbonate banks where NEC can be greater than NEP (Mackenzie et al. 2005). Thus, for many ocean margins, R_{CO2} is primarily determined by the difference between the net DIC transport flux (inputs − outputs) and NEP.

Exchanges across the air-sea interface act by opposing or compensating the net change in DIC and force the system toward equilibrium with the atmosphere (Bauer et al. 2013, Cai 2011, Cao et al. 2020, Dai et al. 2013). Land-derived inputs originate from upland soils (Regnier et al. 2013b) and also from adjacent coastal marsh-estuarine systems (Cai 2011). At the ocean margin-open ocean interface, cross-shelf/slope transport provides a primary exchange pathway, quantification of which, however, remains difficult (e.g., Bauer et al. 2013). Conceptualizations that include the myriad processes and mechanisms contributing to the coastal carbon cycle have been developed (**Figure 1*b***), but quantification of processes is often based on individual case studies (e.g., Bauer et al. 2013, Cao et al. 2014, Dai et al. 2013).

The coastal ocean carbon cycle is further complicated by anthropogenic perturbations that act across the land-ocean continuum and evolve over time (e.g., Mackenzie et al. 2005, Regnier et al. 2013b). During preindustrial times, the coastal ocean may have acted as a net source of atmospheric CO_2 (e.g., Aricò et al. 2021, Bauer et al. 2013, Mackenzie et al. 2004). However, analysis of recent global coastal ocean simulations suggested that the coastal ocean was a small net preindustrial sink of atmospheric CO_2 (Bourgeois et al. 2016, Lacroix et al. 2021a). Regnier et al. (2013b) developed an intermediate view of a near-neutral coastal ocean carbon sink prior to significant human perturbations by assuming that the coastal ocean perturbation scaled to that of the open ocean. These authors also proposed that anthropogenic perturbations originate from increased land-to-ocean carbon inputs, rather than only from atmospheric uptake. However, with increasing atmospheric CO_2 levels, it is anticipated that the future coastal ocean will take up more anthropogenic CO_2 from the atmosphere and export more DIC to the open ocean, at least before carbon emissions reach their peak (Bauer et al. 2013, Bourgeois et al. 2016).

Net-zero carbon emission: achieving an overall balance between CO_2 emissions produced and removed from the atmosphere

Carbon dioxide removal: anthropogenic activities removing CO_2 from the atmosphere and durably storing it in geological, terrestrial, or ocean reservoirs, or in products

Advances have been made in development and implementation of models to investigate coastal carbon cycling processes. Yet, modeling the coastal ocean at global scales remains difficult because of the paucity of observations for model evaluation and the heterogeneity of coastal systems, both of which affect the ability to adequately represent global-scale coastal processes (Hofmann et al. 2011, Holt et al. 2009). So far, only regional models allow inclusion of region-specific biogeochemical processes representative of the spatial and temporal variability. Reconciling and combining results from global and regional models is an important step toward developing the predictive capability that is needed to inform policies aimed at net-zero carbon emission (i.e., achieving an overall balance between CO_2 emissions and that removed from the atmosphere) by the mid-century, which likely will include the implementation of some types of land- and/or ocean-based carbon dioxide removal (CDR) techniques. The implementation of CDR techniques will potentially lead to further and rapid alterations of the global carbon cycle, including the coastal carbon cycle, that will be superimposed on the changes that have already occurred since the start of the industrial period and are expected to continue in the future. Understanding the response of the coastal ocean carbon to such changes poses a grand challenge, which requires careful observational and modeling assessment at both regional and global scales.

Critical knowledge gaps remain in understanding and quantifying coastal carbon fluxes and the underlying controls. These include internal process interactions, responses to external and boundary forcings, and responses to human-induced local and global perturbations. This review provides an analysis of the current qualitative and quantitative understanding of the coastal ocean carbon cycle, with a focus on the air-sea CO_2 exchange, at regional to global scales. It includes novel findings obtained using the full breadth of methodological approaches, from observation-based studies and advanced statistical methods to conceptual and theoretical frameworks, and numerical modeling. Most importantly, it provides a critical review of the current status of coastal ocean carbon research, pointing to the major gaps and challenges that give rise to opportunities for future research.

2. SYNTHESIS OF REGIONAL AIR-SEA CO_2 FLUXES

Assessment of the global coastal ocean air-sea CO_2 flux has advanced significantly over the past four decades. Tsunogai et al. (1999) extrapolated a case study from the East China Sea (ECS) to derive a carbon sink of -1 Pg C year^{-1} for the global continental margin. A subsequent North Sea case study was also extrapolated to the global scale, resulting in a smaller carbon sink of -0.4 Pg C year^{-1} (Thomas et al. 2004). These studies highlighted the importance of the coastal ocean but showed that individual coastal systems vary considerably (Cai & Dai 2004). This motivated more advanced global synthesis efforts based on compilations of local and regional CO_2 flux measurements and province-based extrapolations (e.g., Borges 2005, Cai et al. 2006, Chen & Borges 2009, Chen et al. 2013, Dai et al. 2013, Laruelle et al. 2010).

2.1. New Data Synthesis

A new synthesis of the global coastal ocean CO_2 flux, based on reported region-based integrated CO_2 flux estimates from 1998 until the present, is provided here with detailed methodological explanations given in **Supplemental Material Section 2**. This new synthesis includes 214 regional CO_2 flux estimates in coastal systems (**Figure 2**; **Supplemental Figure 1.1**; **Supplemental Table 1**) with uncertainty and caveats considered (**Supplemental Material Section 2.2**) and is based on regional studies that provided sufficient information to allow recalculation of the gas transfer velocity using the relationships given in Wanninkhof et al. (2013) or Wanninkhof (2014). The calculated CO_2 flux estimates were allocated into 46 MARgins and CATchment Segmentation

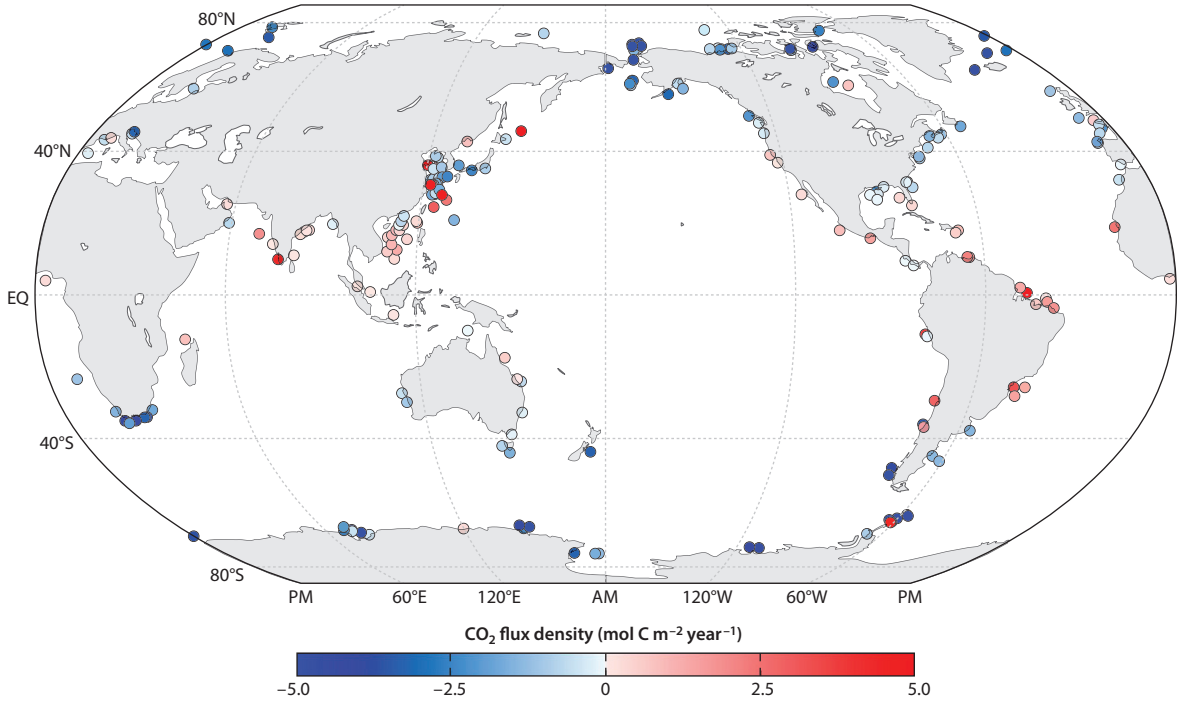

Figure 2

Updated sea-air CO_2 flux density (mol C m^{-2} $year^{-1}$) in the global coastal oceans. Individual sites and associated calculations are detailed in **Supplemental Table 1**.

units, a widely accepted segmentation of the global coastal ocean, the geographical boundaries of which were obtained from Laruelle et al. (2013) with slight modifications, and further categorized into seven major shelf classes (**Supplemental Figure 1.1**) based on the characteristics given in the **Supplemental Material Section 1**.

The new synthesis of air-sea CO_2 fluxes shows an integrated air-sea CO_2 flux (a sink) in the global coastal ocean of -0.25 ± 0.05 Pg C $year^{-1}$, which is within the range of -0.45 to -0.19 Pg C $year^{-1}$ reported in previous studies (Borges et al. 2005, Chen & Borges 2009, Chen et al. 2013, Laruelle et al. 2014, Roobaert et al. 2019). The polar (-134 Tg C $year^{-1}$) and subpolar (-108 Tg C $year^{-1}$) regions contribute the majority to the global sink (**Figure 3**), followed by the western boundary current (WBC) systems (-17 Tg C $year^{-1}$), marginal seas (-11 Tg C $year^{-1}$), and eastern boundary current (EBC) systems (-4 Tg C $year^{-1}$). The tropical (17 Tg C $year^{-1}$) and Indian Ocean (9 Tg C $year^{-1}$) margins are weak sources (**Figure 3**).

The bulk of the CO_2 uptake translates into a globally averaged CO_2 flux density of -0.68 ± 0.14 mol C m^{-2} $year^{-1}$, which suggests that the coastal ocean is a more efficient CO_2 sink relative to the value of -0.5 mol C m^{-2} $year^{-1}$ estimated for the open ocean (Wanninkhof et al. 2013). This flux density represents the lower bound of previously reported ranges [-0.71 mol C m^{-2} $year^{-1}$ (Cai et al. 2006); -1.09 mol C m^{-2} $year^{-1}$ (Chen et al. 2013); -0.73 mol C m^{-2} $year^{-1}$ (Laruelle et al. 2014)], but is only slightly higher than the value of -0.58 mol C m^{-2} $year^{-1}$ reported in the recent assessment by Roobaert et al. (2019), considering the associated uncertainty in both estimates and distinct methodological approaches. Here, we assess fluxes from a literature review of regional studies while Roobaert et al. (2019) applied a neural-network interpolation technique

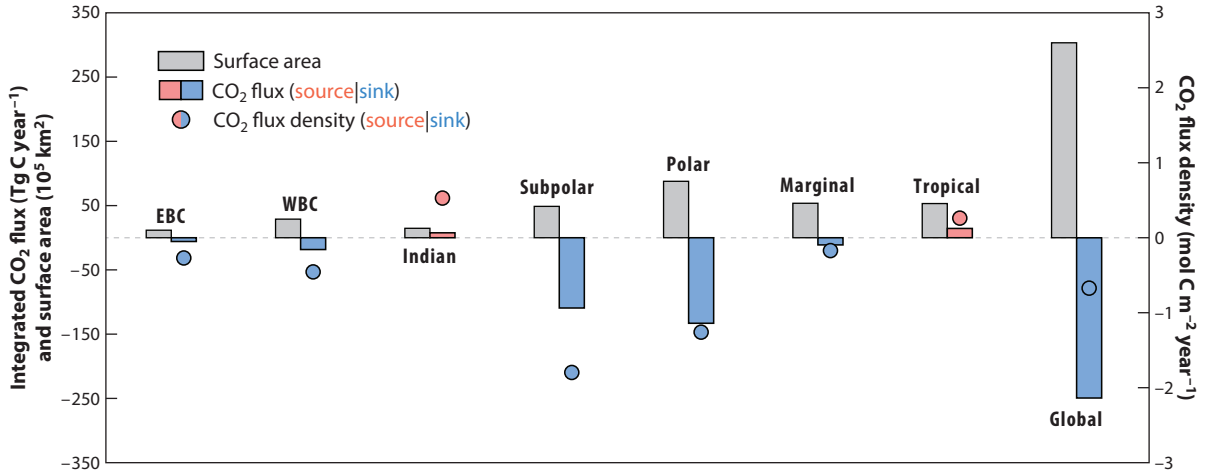

Figure 3

The shelf surface area (*gray bars*), CO_2 flux density (*colored circles*), and spatially integrated CO_2 flux (*red* and *blue bars*) estimated for the seven shelf classes and global shelves. Abbreviations: EBC, eastern boundary current; Indian, Indian Ocean margins; marginal, marginal sea; WBC, western boundary current.

to the CO_2 data gathered in the Surface Ocean CO_2 Atlas (SOCAT) version 4 product (Bakker et al. 2016). Both assessments show a consistent pattern in terms of defining sinks and sources of the seven shelf classes. The larger CO_2 flux obtained from the present synthesis relative to the results of Roobaert et al. (2019) can be attributed to the higher CO_2 flux densities obtained for polar (−1.27 versus −0.75 mol C m^{-2} year^{-1}) and subpolar (−1.80 versus −1.23 mol C m^{-2} year^{-1}) regions and the larger shelf surface areas of 88 × 10^5 versus 81 × 10^5 km^2 in polar and 50 × 10^5 versus 47 × 10^5 km^2 in subpolar regions (surface area estimates are detailed in the **Supplemental Material Section 2.1** and **Supplemental Table 1**). The total differences (−100 Tg C year^{-1}) of the CO_2 sinks in polar (−134 versus −74 Tg C year^{-1}) and subpolar (−108 versus −69 Tg C year^{-1}) regions account for 40% and 51% of the global coastal CO_2 flux derived in this study (−0.25 Pg C year^{-1}) and that of Roobaert et al. (2019) (−0.20 Pg C year^{-1}), respectively.

2.2. Seasonality and Latitudinal Pattern

The latitudinal pattern in the coastal CO_2 flux described by Laruelle et al. (2014) also showed the seasonality of the flux. In this study, the highest CO_2 uptakes were found at high latitudes, followed by moderate uptake at mid-latitudes (Laruelle et al. 2014). At low latitudes, seasonally alternating uptake and outgassing of CO_2 resulted in low net annual air-sea exchanges. This study recognized the large contribution of Arctic and sub-Arctic shelves in the global coastal ocean carbon budget. Seasonal dynamics of the CO_2 fluxes are evident in the mid- and high latitudes of the Atlantic Ocean, showing an atmospheric CO_2 sink in spring, a strong source in summer, and a gradual decrease over fall and into winter (Signorini et al. 2013). This seasonality is mostly driven by changes in sea surface temperature (SST) and NEP. Roobaert et al. (2019) similarly showed CO_2 flux amplitudes that were large at high latitudes, moderate at mid-latitudes, and low at low latitudes (**Figure 4*a***).

The large and consistent uptake of atmospheric CO_2 in polar and subpolar regions was also found in this synthesis (**Figure 3**). The largest variability occurs in the mid-latitudes. At low latitudes, the CO_2 fluxes vary from near neutral to positive (sources of atmospheric CO_2). A striking

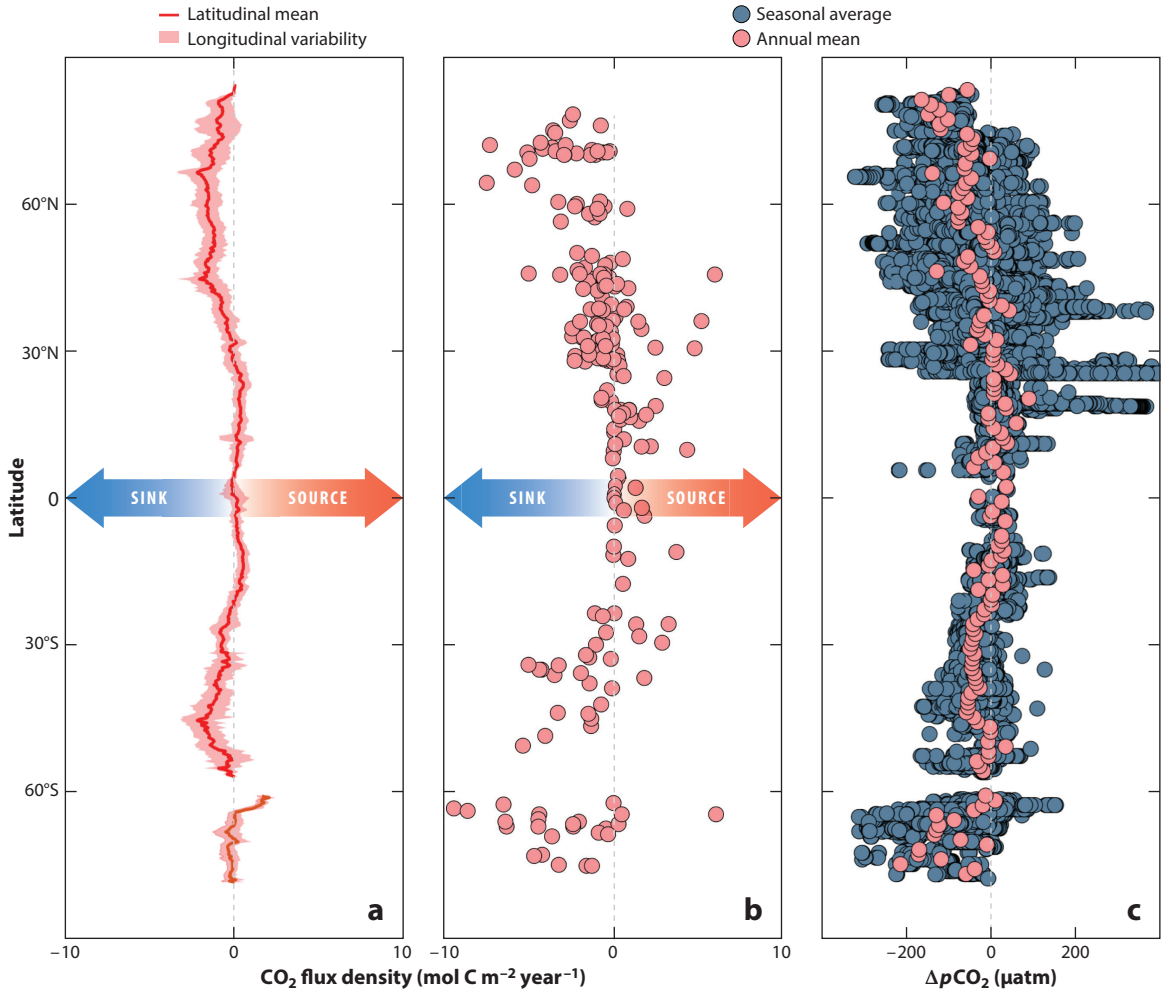

Figure 4

Latitudinal distributions of (*a*) annual CO_2 flux density reported by Roobaert et al. (2019), (*b*) annual CO_2 flux density obtained from compilation of data presented in the literature, and (*c*) seasonal and annual averages ΔpCO_2 (difference of pCO_2 between seawater and the atmosphere) at a distance of 50 km from the major land masses. Abbreviation: pCO_2, partial pressure of CO_2.

contrast is that the literature-based estimates have a more pronounced dynamic range than that shown in **Figure 4*a***.

The latitudinal distribution of SST, sea surface partial pressure of CO_2 (pCO_2), and ΔpCO_2 (defined as the difference in pCO_2 between the sea and the air) based on SOCAT product (version 2021) (**Figure 4*c***; **Supplemental Figure 2.3**) at three different distances—50, 100, and 200 km (**Supplemental Figures 2.4–2.6**)—away from the global shoreline provide further characterization of the global pattern, similar to the analysis in Cao et al. (2020). The ΔpCO_2, indicative of the air-sea CO_2 fluxes, is similar to the global pattern based on our literature synthesis (**Figures 4*a*,*b***), but with a larger dynamic range. This larger dynamic range is even more evident for the seasonal data (blue dots in **Figure 4*c***), relative to the annual mean, suggesting strong seasonal heterogeneity in CO_2 fluxes at the same latitudes and along latitudes.

River-dominated ocean margin: the coastal system of which CO_2 fluxes are dominated by riverine inputs of carbon and nutrients at the land-ocean margin interface

Ocean-dominated margin: the coastal system of which CO_2 fluxes are dominated by oceanic inputs of carbon and nutrients at the ocean margin-open ocean interface

The pCO_2 and ΔpCO_2 have a less defined latitudinal pattern during each season than that of SST (**Supplemental Figures 2.4–2.6**). The pCO_2 is low at mid- and high latitudes and slightly higher in tropical zones. The spatial variance of pCO_2 at 50 km is large at latitudes that are influenced by upwelling and terrestrial input, and shows considerable seasonal variability. Also, summer pCO_2 drawdown is pronounced at high latitudes due to biological CO_2 consumption. In autumn, the latitudinal pattern of pCO_2 is not as clear. Seasonal changes in pCO_2 are smaller for data collected at greater distance offshore (i.e., at 200 km), with the majority of values around 400 μatm (**Supplemental Figures 2.4–2.6**). The 200-km spatial and temporal distribution patterns are rather similar to those expected for the open ocean, and the ΔpCO_2 latitudinal pattern is similar to that of sea surface pCO_2.

The preceding description suggests that both thermal and nonthermal drivers control the latitudinal pCO_2 and the associated fluxes, as previously reported (Cao et al. 2020). The effect of temperature increases toward the equator, where increasing SST elevates the surface seawater pCO_2. Nonthermal factors, such as water mass mixing with open ocean waters (e.g., upwelling), and local biological alterations (e.g., higher biological productivity at mid- and high latitudes, and lower productivity but higher riverine organic matter input at low latitudes) are superimposed on the thermal control pattern (Cao et al. 2020, Chen et al. 2013).

The relative importance of thermal and nonthermal factors on coastal CO_2 dynamics and fluxes was further assessed for interseasonal pCO_2 changes using the approach given in Cao et al. (2020). With this approach, the observed interseasonal pCO_2 change is decomposed into a temperature-controlled change and a non-temperature-controlled residual. The main controls of interseasonal pCO_2 changes in different latitudinal bands during seasonal transitions differ. However, the interseasonal changes of global coastal ocean pCO_2 are generally more determined by nonthermal factors rather than temperature, which is supported by a statistically significant positive relationship between the total change and nonthermal factors (**Supplemental Figure 2.7**).

3. OCEAN-DOMINATED MARGINS VERSUS RIVER-DOMINATED OCEAN MARGINS

The previously developed framework that categorizes river-dominated ocean margin (RiOMar) and ocean-dominated margin (OceMar) systems allows conceptualization of coastal ocean carbon cycle processes (Cao et al. 2020, Dai et al. 2013). Both systems are characterized by interactive exchanges and transport at the boundaries along the river-estuary-shelf-ocean continuum and intrinsic biogeochemical reactions that determine the air-sea CO_2 flux. However, the distinction recognizes differences in controls on CO_2 fluxes and carbon cycling in coastal systems that are dominated by riverine inputs at the land-ocean margin interface versus those that are dominated by oceanic inputs at the ocean margin-open ocean interface (Cao et al. 2020, Dai et al. 2013).

A theoretical framework was developed to resolve the CO_2 source/sink nature of OceMar systems (**Supplemental Material Section 3.1**), such as systems affected by boundary currents and coastal upwelling, and RiOMar systems, such as river plume-shelf systems receiving large terrestrial loads. In OceMar systems, DIC and nutrients, supplied by the open ocean and distributed by the three-dimensional circulation, are transported to the ocean margin and subsequently upwelled or mixed into the euphotic zone, where the nutrients support enhanced primary production. Changes in DIC relative to nutrients, both transformed by physical transport and biological processes, determine whether there is an excess or deficit in DIC. Excess DIC in seawater is eventually released to the atmosphere, making the ocean margin a source of atmospheric CO_2, whereas a DIC deficit is compensated by input of atmospheric CO_2 making the

region a CO_2 sink (Cao et al. 2020, Dai et al. 2013). In RiOMar systems, the DIC and nutrients originating from land or rivers are delivered to nearshore waters via estuarine/bay circulation and subsequently exported to the continental shelf via wind-driven circulation of the low saline river plume (Gan et al. 2009). The balance between the externally sourced DIC and nutrients and internal biogeochemical interactions thus controls the CO_2 fluxes (Cao et al. 2020).

Diatom-diazotroph assemblages: a widespread marine planktonic symbiosis between diatoms and N_2-fixing bacteria or prokaryotes

The RiOMar and OceMar designations are spatially and temporally variable and can be interchangeable. Thus, a RiOMar can shift to an OceMar depending on the relative inputs of water and biogeochemical compounds across the land-ocean margin and ocean margin-open ocean interfaces and the intensity of the physical forcing that regulates these inputs. A decrease in river discharge during dry seasons constrains the spatial scale of river plumes, potentially converting a RiOMar to an OceMar, particularly if coastal upwelling or vertical mixing is strengthened by the interaction between wind-driven shelf currents and topography.

3.1. River-Dominated Ocean Margin Systems: Characteristics and Diagnosis

Buoyant surface plumes that extend from large rivers and estuaries into the coastal ocean are characteristic of RiOMar systems. Estimates of the plume area associated with the world's 19 largest rivers showed a total annual mean plume area of 3.7×10^6 km^2 (Kang et al. 2013), accounting for ~14% of the total continental shelf area worldwide. Extrapolation of the CO_2 flux density in river plumes of the Amazon, Changjiang, Mississippi, and Loire Rivers indicates a global CO_2 sink for large river plumes of about -0.066 Pg C year^{-1}, contributing to ~25% of the global continental shelf CO_2 sink (Cai et al. 2014). The hydrodynamics of individual plumes are complex and heterogeneous. The Amazon River plume flows northwestward and can be partly carried eastward by retroflection of the North Brazil Current to feed into the North Equatorial Countercurrent (Ibanhez et al. 2016). The Mississippi-Atchafalaya River plume propagates offshore toward the remote southern Gulf of Mexico (Schiller & Kourafalou 2014). The Mekong River plume discharged into the South China Sea (SCS) can also veer into the deep SCS basin via coastal jet separation (Gan & Qu 2008).

Mixing of seawater with riverine freshwater dominates pCO_2 dynamics in river plumes by altering the carbonate chemistry. High bicarbonate (HCO_3^-) concentrations in subtropical to mid-latitude river waters (e.g., the Changjiang, Mississippi, and Pearl Rivers) exhibit a stronger buffering capacity to changes in pCO_2 than that of tropical river waters (e.g., the Amazon and Orinoco Rivers) with lower HCO_3^- concentrations (Cai et al. 2014). The pCO_2 in HCO_3^--rich river waters therefore decreases gradually along the plume, while in HCO_3^--poor river waters it decreases rapidly in the near field of the plume and approaches the seawater pCO_2 at the plume front.

River plume pCO_2 dynamics are further affected by biological processes that depend on the trade-off between degradation of terrestrial organic matter and riverine nutrient-enhanced primary production. Along a river plume, the sea surface often shifts from a source of atmospheric CO_2 in the near field, due to organic matter degradation and excess CO_2 inherited from the river, to a sink as a result of enhanced biological removal of CO_2 (Huang et al. 2015). The biologically mediated low pCO_2 surface water is transported away from estuaries because the air-sea pCO_2 equilibrium time is often much longer than the residence time of the plume or surface waters (Zhao et al. 2021). In the high-salinity far field, the sea surface tends to be in a near-neutral state due to weakened phytoplankton production resulting from depleted nutrients, and temperature becomes the dominant control on the surface pCO_2 and air-sea CO_2 flux. However, for some systems, such as the Amazon and Mekong River plumes, nitrogen fixation by diatom-diazotroph assemblages can supply nutrients that sustain the biological pump in the outer plume.

In addition to the analysis for the Pearl River plume (Cao et al. 2020), the carbon dynamics of the RiOMar systems represented by the Mekong River plume and the Mississippi-Atchafalaya River plume were assessed using the theoretical diagnostic framework (**Supplemental Material Section 3.1**; **Supplemental Figure 3.1*a*,*b***). The Mekong River discharge has relatively high nutrient concentrations, greater than 40 μmol L^{-1} of nitrate + nitrite ($NO_3 + NO_2$) and ∼1 μmol L^{-1} of phosphate (PO_4), that support new production in the SCS (Grosse et al. 2010). Similarly to the Amazon River plume, the Mekong River plume is influenced by N_2 fixation potentially by diatom-diazotroph assemblages with rates up to 0.55 μmol N L^{-1} day^{-1}, which accounts for 1–47% of the primary production nitrogen demand (Grosse et al. 2010).

The diagnostic approach estimate for DIC consumption fueled by riverine nutrients in the Mekong River plume is 7.9 ± 2.4 μmol kg^{-1} ($NO_3 + NO_2$ based) or 2.7 ± 0.6 μmol kg^{-1} (PO_4 based), resulting in high δDIC^* (changes in the DIC concentration solely induced by air-sea CO_2 exchange as explained in **Supplemental Material Section 3**) values of 31 ± 7 μmol kg^{-1} based on $NO_3 + NO_2$ and 37 ± 10 μmol kg^{-1} based on PO_4 in the surface plume (salinity < 33.5) in late summer of 2007 (**Supplemental Figure 3.2**). The DIC consumption fueled by N_2 fixation can offset at most 47% of the δDIC^*. The Mekong River plume is therefore a source of atmospheric CO_2, having already released CO_2 to the atmosphere over the timescale considered by the framework with sea surface pCO_2 decreasing from ∼500 μatm before air-sea exchange to ∼379 ± 15 μatm at measurements, almost equilibrating with the atmospheric pCO_2 of ∼381 μatm.

The Louisiana shelf in the northern Gulf of Mexico annually receives ∼0.7–1.0 Tg N of nitrate (Lehrter et al. 2013) and ∼17 Tg C of HCO_3^- from the Mississippi-Atchafalaya River system (Lohrenz et al. 2013). Although highly supersaturated pCO_2 values were observed in narrow regions near river mouths, the inner shelf influenced by the riverine inputs remained largely undersaturated with respect to the atmospheric CO_2 (Huang et al. 2015). The diagnostic result for the Mississippi-Atchafalaya River plumes (salinity < 35) in early summer of 2006 (**Supplemental Figure 3.3**) shows that primary production consumes DIC by 232 ± 110 μmol kg^{-1} based on $NO_3 + NO_2$, lowering the seawater pCO_2 to less than 100 μatm. The spatially averaged δDIC^* is −67 ± 56 μmol kg^{-1}, indicating a strong deficit of DIC, which can explain its behavior as a sink of CO_2 over the inner shelf with a ΔpCO_2 of −125 ± 75 μatm.

3.2. Ocean-Dominated Margin Systems: Characteristics and Diagnosis

For OceMar systems, the material exchange across the ocean margin-open ocean interface is poorly known and is dependent on the diverse geomorphology and ecosystems that characterize these systems. Quantifying this exchange at regional or global scales is challenging because of the lack of clearly defined boundaries, insufficient understanding of associated processes such as boundary current intrusions, cross-slope dynamics, and exchanges induced by meso- and submesoscale oceanic processes (Dai 2021, and references therein).

3.2.1. Eastern boundary current systems. The EBC systems and other coastal upwelling systems are dependent on inputs of oceanic-derived nutrients to sustain their high biological productivity (Wollast 1991). The California Current System, an example of an EBC upwelling system (**Supplemental Material Section 1**; **Supplemental Figure 3.4*a***), transports DIC- and nutrient-enriched subsurface waters, derived from offshore deep oceanic waters, across the shelf to the nearshore surface waters (Cai et al. 2020). The upwelling brings water from 150–200 m to the surface, resulting in pCO_2 levels that can reach 1,000 μatm. This water is then transported seaward and southward while the pCO_2 is drawn down by biological productivity to ∼200 μatm, far below the atmospheric pCO_2 value (Feely et al. 2008). Such a pronounced decrease in seawater

pCO_2 occurs because complete utilization of preformed nutrients in upwelled waters exceeds the corresponding net DIC consumption, which has been diagnosed semiquantitatively (Cao et al. 2014). Controls of the CO_2 flux in other EBC systems in which the majority of DIC and nutrients in the upper layer originate from locally wind-induced cross-shelf transport of the nonlocal deep waters in the subtropical gyre of the open ocean are likely similar. Depending on the DIC/nutrient ratios in source waters, CO_2 flux density can vary, but the DIC deficit relative to that of nutrients makes the system a sink of atmosphere CO_2 (Section 2).

3.2.2. Western boundary current systems. The WBC systems are typically found along coastal margins with wide shelves. The outer and mid-shelf dynamics are dominated by inputs from the open ocean. The ECS (**Supplemental Figure 3.4*e***), a OceMar system, is characterized by intrusions of warm, high-salinity, and high-nutrient waters onto the outer shelf that are derived from the Kuroshio, a WBC in the western North Pacific (WNP) (Guo et al. 2015, Liu & Gan 2012). Zhang et al. (2019) estimated that the Kuroshio contributes 72% and 84% of external inputs of dissolved inorganic nitrogen (DIN) and phosphorus (DIP), respectively, to the entire ECS shelf, supporting 50% of DIN-based primary production and 61% of DIP-based primary production. Budget analysis showed that the total influx of DIC (75 Tmol C $year^{-1}$) from the intrusion of Kuroshio waters into the ECS exceeded the DIC consumption fueled by the Kuroshio-sourced DIN (0.15 Tmol N $year^{-1}$) and DIP (0.011 Tmol P $year^{-1}$) (Chen & Wang 1999). However, the biological consumption of open ocean–sourced DIC produces a deficit relative to nutrient use, causing the outer ECS to behave as a sink for the atmospheric CO_2 (Guo et al. 2015).

3.2.3. Marginal seas. Semi-enclosed marginal seas are characterized by complex transport pathways and lateral and vertical fluxes/exchanges with water masses of relatively longer residence times that allow for biogeochemical transformations. Using a simple one-dimensional advection-diffusion model, Dai et al. (2013) showed that the DIC and nutrient inputs from upwelling of the deep Pacific water provided via the SCS overflow result in excess DIC. The DIC excess relative to open ocean–sourced nutrients, as diagnosed previously (Cao et al. 2020, Dai et al. 2013), is eventually released to the atmosphere. Chou et al. (2017) adopted this approach to explain the occurrence of atmospheric CO_2 source areas within the Japan/East Sea in summer that are supported by CO_2 sources from the adjacent open ocean.

The Caribbean Sea is the largest marginal sea of the Atlantic Ocean (**Supplemental Figure 3.4*b***) and experiences overflow from the Atlantic similar to that from the WNP into the SCS, but with a more complex circulation pattern (MacCready et al. 1999). Mid-depth water, which is sourced from Upper North Atlantic Deep Water, flows from the Atlantic into the Virgin Islands basin, and then over the Jungfern-Grappler complex into the eastern Caribbean (MacCready et al. 1999). This sole source of water for the deep Caribbean is presumably balanced by diffusively driven upwelling elsewhere in the basin (Ribbat et al. 1976). Upward water displacement exists in the deep layer (Gallegos 1996), induced by renewal flows across the deepest passages, that supplies both DIC and nutrients to the surface mixed layer, where the relative CO_2 consumption/release determines whether this OceMar system acts as a CO_2 source or sink (Dai et al. 2013). Samples collected in April 2021 showed δDIC^* values of 1.4 ± 2.5 μmol kg^{-1} and ΔpCO_2 of 3 ± 5 μatm (**Supplemental Figures 3.1*c*, 3.5**), further demonstrating that the Caribbean Sea is nearly in equilibrium with the atmospheric CO_2.

3.2.4. Indian Ocean margins. The Arabian Sea on the western Indian Ocean margin is an OceMar system with intrusion of deep waters from the Indian Ocean onto the continental margin via horizontal advection, which are then transported upward via vertical mixing and upwelling (Valsala & Murtugudde 2015) (**Supplemental Figure 3.4*f***). During the southwest monsoon

season when wind-driven coastal upwelling frequently occurs, high primary production is often observed (Brand & Griffiths 2009). Cao et al. (2020) estimated positive PO_4-based δDIC^* values during all seasons (~23 μmol kg^{-1} in winter, summer, and autumn and ~4 μmol kg^{-1} in spring), suggesting that the Arabian Sea acts as a weak source of CO_2 to the atmosphere.

3.3. Arctic Margins

Arctic continental shelves are influenced by both river inputs and exchanges with the Pacific and Atlantic Oceans (Roeske et al. 2012, Terhaar et al. 2021). The large influx of freshwater from riverine inputs makes the Arctic Ocean well stratified with a distinct surface layer of reduced salinity (Abrahamsen et al. 2009). The Arctic Ocean also receives inflows from the Atlantic and Pacific Oceans via the Greenland-Scotland Ridge (Hansen et al. 2008) and Fram Strait and the Barents Seas Opening, respectively (e.g., Beszczynska-Möller et al. 2012, Ingvaldsen et al. 2002, Schauer et al. 2004).

The Bering Sea (**Supplemental Figure 3.4*c***) provides an example system for analyzing possible controls on the air-sea exchanges featuring both riverine input and exchanges with the open ocean (Aiello & Ravelo 2012). As such, the Bering Sea is intermediate between OceMar and RiOMar systems, with surface pCO_2 and CO_2 fluxes characterized by large spatial-temporal variability and diverse controlling processes. In spring and summer, the Bering Sea shelf is undersaturated with respect to atmospheric pCO_2 mainly because of biological production (Bates et al. 2011, Chen et al. 2004). However, Sun et al. (2020) observed that in summer the central Bering Strait is supersaturated with respect to the atmospheric pCO_2 as a result of upwelling. In contrast, the Bering Sea basin and eastern nearshore regions are a neutral or weak CO_2 sink, as a result of the high nutrients/low chlorophyll status and riverine input, respectively. Chen (1985) suggested that in winter the Bering Sea shelf was a potential sink for atmospheric CO_2 due to cooling, while Kelley & Hood (1971) and Cross et al. (2014) found supersaturation of pCO_2 in winter in the Bering Sea shelf area.

The Alaskan Stream flows into the Bering Sea and transports relatively warm water in the surface layer. This water mixes with the dichothermal water from ~150 m that forms during the winter and warm subsurface Alaskan Stream (depth of ~300 m) via eddy-induced upwelling and along tilted-up isopycnals (Miura et al. 2002, Mizobata et al. 2002). Using data collected in October 2007 in the eastern Bering Sea basin, the diagnostic approach estimated that biological production consumed 2.0 ± 0.6 μmol kg^{-1} $NO_3 + NO_2$, equivalent to a DIC consumption of 13.1 ± 4.0 μmol kg^{-1} (**Supplemental Figures 3.1*d*, 3.6**). The resultant δDIC^* is 1.5 ± 1.8 μmol kg^{-1}, indicating a neutral or weak CO_2 sink for the Bering Sea basin in autumn. However, the dominant controls on the CO_2 source/sink nature for the entire Bering Sea (including shelf and basin regions) in all seasons warrant further examination.

4. THREE REGIONAL CASE STUDIES ON SPATIAL AND SEASONAL VARIABILITY AND LONG-TERM TRENDS OF SEA SURFACE pCO_2: THE BALTIC SEA, THE MID-ATLANTIC BIGHT, AND THE SOUTH CHINA SEA

The Baltic Sea (BS), the SCS, and the Mid-Atlantic Bight (MAB) (**Supplemental Figure 4.1**) are regions with long-term sea surface pCO_2 measurements at high spatio-temporal resolution that allow estimates of air-sea CO_2 fluxes and characterization of biogeochemical transformations (**Figure 5**). In addition, coupled circulation-biogeochemical models have been implemented to investigate carbon cycling dynamics in these three regions (for additional information, see **Supplemental Material Section 4**).

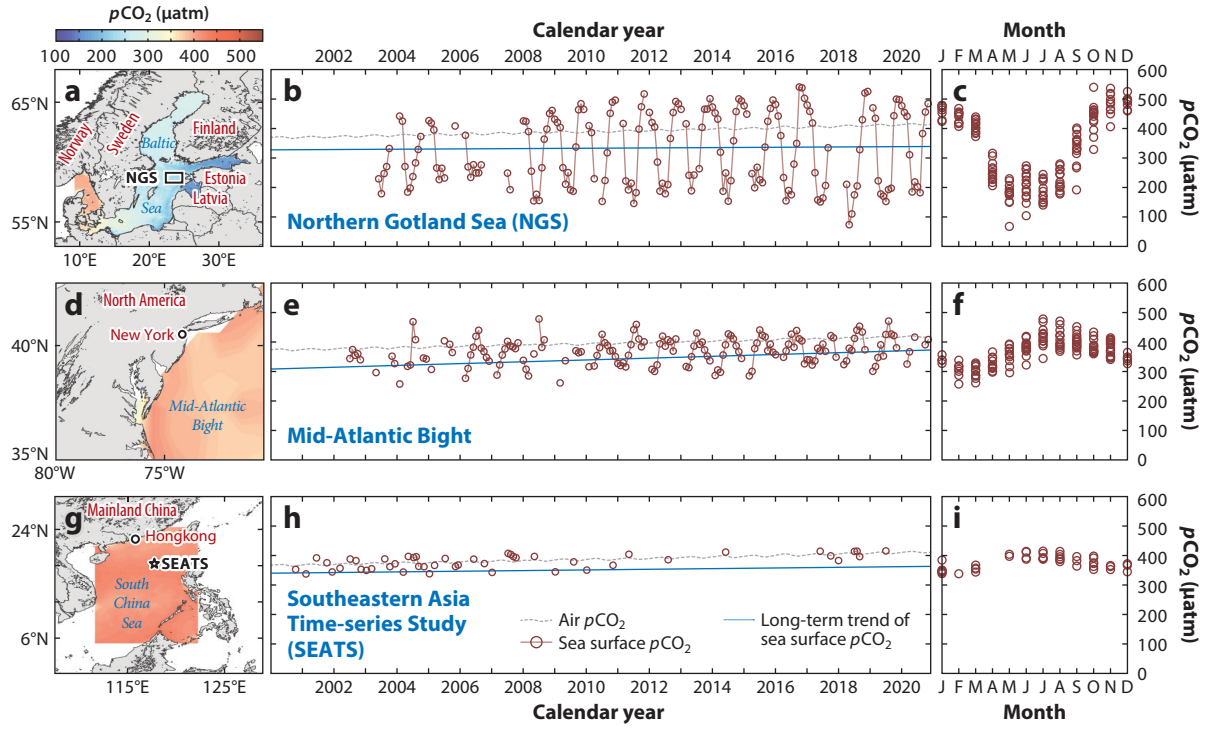

Figure 5

Spatial, long-term, and seasonal variability of sea surface pCO_2 in (*a–c*) the BS, (*d–f*) the MAB, and (*g–i*) the SCS. The spatial distribution of sea surface pCO_2 (*a*,*d*,*g*) represents Northern Hemisphere summer conditions and is based on remote sensing–supported pCO_2 estimates from the climatological monthly average of August (2002–2011) with a horizontal resolution of 0.0417° × 0.0417° for the BS (Zhang et al. 2021), a spatial interpolation of the gridded summer data (1° × 1°, SOCAT version 2021) for the MAB, and reconstructed data (0.5° × 0.5°) for the SCS with relatively high reliability (**Supplemental Figure 2.2**) (Wang et al. 2021). The air pCO_2 data (*b*,*e*,*h*) were obtained from the Mauna Loa Observatory (Keeling et al. 2005). The monthly averaged sea surface pCO_2 data for the BS (*b*,*c*) were calculated from cruise averages of each crossing of the NGS as shown in Schneider & Müller (2018). The MAB data (*e*,*f*) are based on monthly gridded data from SOCAT version 2021 (1° × 1°) as shown in Xu et al. (2020). The SCS data (*b*,*i*) are based on time-series measurements at the SEATS station (116°E, 18°N) in the northern basin of the SCS according to Sheu et al. (2010) and Dai (unpublished data). The long-term trends of sea surface pCO_2 are based on a linear regression fit to the seasonally detrended monthly mean values (*b*,*e*,*h*). Abbreviations: BS, Baltic Sea; MAB, Mid-Atlantic Bight; NGS, Northern Gotland Sea; pCO_2, partial pressure of CO_2; SCS, South China Sea; SEATS, Southeastern Asia Time-series Study; SOCAT, Surface Ocean CO_2 Atlas.

The BS, a semi-enclosed marginal sea, can be considered one of the world's largest estuaries subjected to perturbation by anthropogenic activities, notably by eutrophication. Among the three case study sites, the BS has the largest spatial variability [standard deviation (SD) ~55.1 µatm in summer (**Figure 5*a***)] and the strongest seasonality of sea surface pCO_2 [(mean amplitude defined as the difference between the highest and the lowest monthly mean pCO_2 across all years ~319.3 µatm (**Figure 5*c***)]. Primary production and mineralization processes have been identified as the main drivers for the seasonality of sea surface pCO_2 (Schneider & Müller 2018). The MAB, located on the North American East Coast, is characterized by a broad, shallow shelf with moderate riverine inputs discharged through large estuaries. The MAB shows intermediate spatial [SD ~32.3 µatm in summer (**Figure 5*d***)] and seasonal [mean amplitude ~116.6 µatm (**Figure 5*f***)] variability in sea surface pCO_2. The seasonal cycle of pCO_2 in this system is primarily driven by the SST (DeGrandpre et al. 2002, Signorini et al. 2013, Xu et al. 2020). Local biological

production partially counteracts the thermally induced pCO_2 increase during spring and summer, but the overall seasonality is not significantly altered because stratification inhibits the nutrient supply to the surface water. Finally, the SCS, one of the largest marginal seas, is influenced by the Asian monsoons and spans a wide range of biogeographic regimes with characteristic oligotrophy in its basin area. Here, sea surface pCO_2 has the lowest spatial [SD $\sim$ 13.0 μatm in summer (**Figure 5*g***)] and seasonal heterogeneity [mean amplitude $\sim$ 64.3 μatm (**Figure 5*i***)] relative to that observed for the BS and MAB. The heterogeneous nature of pCO_2 and uneven observations in the SCS affect the uncertainty of gridded pCO_2 used in the flux estimate (**Supplemental Figure 2.1**). Controls on the pCO_2 seasonality in the SCS differ among its subregions, but overall it is modulated by SST and mixed layer depth that govern the seasonal nutrient supply from depth (Li et al. 2020b, Yang et al. 2021).

The long-term trends of sea surface pCO_2 differ substantially between the three regions. Synthesis of all available data collected at the Southeastern Asia Time-series Study site (**Figure 5*g***) in the SCS basin shows a long-term increasing trend of 2.5 $\pm$ 1.0 μatm year^{-1} (R^2 = 0.33), based on a linear regression, that is synchronous with the atmospheric pCO_2 level since 2000 (**Figure 5*h***). However, when seasonal variability is removed, this long-term trend is reduced to 1.4 $\pm$ 0.5 μatm year^{-1} (R^2 = 0.45), which is less than the rate of atmospheric pCO_2 increase. In the MAB, the long-term increase in sea surface pCO_2 is 2.4 $\pm$ 0.6 μatm year^{-1} after seasonal detrending, which is comparable to or slightly more than that of $\sim$1.8 μatm year^{-1} for atmospheric CO_2 (**Figure 5*e***). In the BS, the seasonally detrended pCO_2 data show a smaller rate of increase of 0.06 μatm year^{-1} during the period 2003–2020, but associated with a large uncertainty of $\pm$1.02 μatm year^{-1} (**Figure 5*b***). In contrast to the large uncertainty associated with pCO_2 trend analysis, the BS CO_2 system shows a long-term and steady increase in alkalinity that emerged in the mid-1990s (Müller et al. 2016). The amplitude of seasonal variability in sea surface pCO_2 (**Figure 5*c*,*f***) for the BS and MAB is larger than the secular trend, making it difficult to determine a meaningful rate of change on decadal timescales and thus reliably predict the temporal evolution of the respective carbon sinks (for additional information, see **Supplemental Material Section 4**).

5. MODELING COASTAL OCEAN CARBON

Numerical models are capable of examining complex processes in a holistic way and provide an approach for reconstructing historical changes in coastal carbon fluxes, as well as projecting changes into the future (e.g., Bourgeois et al. 2016, Lacroix et al. 2021a, Legge et al. 2020, Siedlecki et al. 2021). Furthermore, numerical models are applied to quantify critical processes that are difficult to constrain through in situ measurements, such as NEP (Gan et al. 2010, Herrmann et al. 2015, Lacroix et al. 2021a) and the cross-shelf and/or cross-interface transfer of carbon (Druon et al. 2010, Yuan et al. 2018). In addition to considering the impacts of climate change and atmospheric CO_2 increase on the coastal carbon cycle, current biogeochemical models also provide assessments of other environmental threats posed by human activities that contribute to eutrophication, acidification, and hypoxia (Fennel & Testa 2019, Laruelle et al. 2017, Li et al. 2020a, Takeshita et al. 2015, Yu et al. 2021) that have direct and indirect consequences for coastal carbon cycling.

Coastal ocean carbon models range from conceptual box (budget) models to three-dimensional coupled circulation-biogeochemical models, some of which include data assimilative capability (e.g., Xiao & Friedrichs 2014). Modeling studies have been successfully conducted in different coastal regions and encompass a range of space and timescales (**Supplemental Table 2**). A common requirement of these models is the need to identify and constrain the processes that control carbon cycling and the flow of organic and inorganic carbon into and out of the coastal system.

Thus, quantification of coastal carbon cycling requires accurate representation of exchanges and fluxes across interfaces with the open ocean, land, atmosphere, and sediment. Equally important are representations of the internal transport and transformations of carbon via circulation and biogeochemical processes (e.g., NEP, heterotrophic respiration, NEC). Current approaches in representing these fluxes and processes, imposed limitations, and the implications for carbon cycling at global and regional scales are highlighted by reviewing representative global and regional models.

5.1. Budgets and Box Models

Carbon budgets constructed for continental margins are based on aggregate approaches that average processes, fluxes, and exchanges in space and time. These mass balance approaches have provided useful insights regarding the magnitude of carbon fluxes and inventories at global and regional scales, with a specific focus on the trophic status of the global coastal ocean and the air-sea CO_2 exchange (e.g., Gattuso et al. 1998, Mackenzie et al. 2005, Smith & Hollibaugh 1993, Wollast 1993). Advances in global coastal carbon budgets are facilitated by observations that constrain key fluxes such as the air-sea CO_2 exchange, the inclusion of overlooked fluxes attributed to coastal vegetated ecosystems (Bauer et al. 2013), and the explicit accounting of the anthropogenic perturbation of land-to-open ocean carbon fluxes (Regnier et al. 2013b). Nevertheless, the outstanding question of whether continental shelves exhibit net autotrophy or heterotrophy remains to be resolved (Bauer et al. 2013).

In parallel with implementation of carbon budget models, conceptual global box models have provided complementary, mechanistic insights into how changes in physical and biogeochemical processes resulting from the combined effects of changing climate, atmospheric composition, and land use may have affected past global carbon fluxes and may indicate impacts on projected future fluxes (Mackenzie et al. 1998, 2000, 2002, 2004). These models are useful in isolating the effects of different stressors on carbon fluxes in the global coastal ocean and allow for a wide range of sensitivity analyses, but considerations of the spatio-temporal heterogeneity arising from complex circulation patterns or widely varying biological activity are not allowed by the model structure.

5.2. Global and Regional Ocean Biogeochemical Models

Coupled three-dimensional physical-biogeochemical models, at either global or regional scales, extend the understanding of coastal carbon processes and fluxes over spatial and temporal scales that go beyond the constraints of box model approaches and limited measurements.

5.2.1. Global ocean biogeochemical models. Global ocean biogeochemical models (GOBMs) (Dunne et al. 2020, Tjiputra et al. 2020), such as those used in the United Nations Intergovernmental Panel on Climate Change (Ciais et al. 2013) or the Global Carbon Project (Friedlingstein et al. 2020), have resolutions that are typically too coarse to provide a reliable basis for the analysis of coastal ocean carbon fluxes (Holt et al. 2009, Mathis et al. 2017). An equally important limitation is that these models do not include or only provide simplistic representations of processes relevant to the coastal ocean interface, such as time-varying riverine fluxes (Lacroix et al. 2020), their modulation by the estuary-coastal vegetation continuum (Bauer et al. 2013), and benthic carbon processing (Bianchi et al. 2021, Krumins et al. 2013). However, improved model resolution, afforded by advances in computational capabilities, allows GOBMs to represent important features of the coastal ocean, such as three-dimensional material and substance transports, residence times (Lacroix et al. 2021a, Liu & Gan 2017), air-sea CO_2 exchange (Bourgeois et al. 2016), and riverine fluxes (Dunne et al. 2020; Lacroix et al. 2020, 2021a,b). Additionally, the biogeochemical

representation of specific coastal processes (e.g., heterotrophic respiration and burial of organic carbon, benthic calcification) greatly lags behind improvements in model resolution.

Downscaled and nested models combine the advantages of the coarse resolution of large-scale global models with high-resolution regional models. Downscaling allows exchange of information between coastal and oceanic domains, thereby maintaining connectivity between oceanic and coastal systems (Mathis et al. 2017, Mayer et al. 2018). The higher-resolution regional model allows detailed representations of processes that are unresolved (e.g., mesoscale and sub-mesoscale circulation) or are system specific (e.g., lower trophic-level structure) in the global model. Two-way nested high-resolution regional models are also capable of providing feedbacks to the global model of coastal information to better predict global carbon cycle. An added benefit is that global models typically provide longer simulations due to their coarse resolution without the need of boundary conditions. Inherent difficulties associated with resolving the fine-scale features of the coastal ocean (e.g., estuarine plumes, coastal fronts) within state-of-the-art global models make regional models essential in assessment of coastal carbon cycling and fluxes and related environmental consequences, such as hypoxia (Fennel & Testa 2019).

5.2.2. Regional ocean biogeochemical models. Regional coastal carbon models represent a diversity of approaches that reflect system understanding and characteristics, and data availability. Regional models have been applied to a wide range of systems (**Supplemental Table 2**) to investigate controls on carbon cycling (e.g., Druon et al. 2010), cross-shelf export (e.g., Fennel & Wilkin 2009, Frischknecht et al. 2018), seasonal and spatial variability in carbon chemistry (e.g., Fennel et al. 2008, Gomez et al. 2020, Turi et al. 2014), and historical trends (e.g., Mathis et al. 2019). Regional models also provide the ability to examine subregional variability that is not easily accessible with global models. Although implemented for a diversity of systems, these models yield common metrics, such as export flux estimates (**Supplemental Table 2**), that have the potential to perform across-system comparisons of the processes controlling coastal carbon cycling.

Estuaries, which function as a filter and/or conduit across the land-ocean interface, have also been modeled at the regional scale using coupled physical-biogeochemical models (Regnier et al. 2013a). To date, only a few modeling studies have partly addressed the catchment-river-estuary-shelf continuum in a single framework (St-Laurent et al. 2020). The inclusion of such linkages across the land-estuarine-ocean continuum is critical for assessing past and future trends in carbon cycling.

Regional carbon cycling models developed for the SCS, the MAB region, and the BS provide a comparison of three contrasting systems and discussions of limitations and implications for model results (**Supplemental Material Section 4**). Simulation of pCO_2 fluxes in these coastal oceans has proven to be difficult and depends on regionally based physical and biological dynamics. In the BS, the lack of simulation of additional nitrogen source (e.g., N_2 fixation or vertical mixing) inhibited reproducing the regional CO_2 flux (Gustafsson et al. 2015) during the period between spring blooms and the accumulation of cyanobacteria in July when nitrogen is depleted (Fransner et al. 2018, Schneider et al. 2014). In the SCS, simulation of the pCO_2 dynamics has proven difficult because of the spatio-temporal patterns of salinity and surface total alkalinity (TA) that partly drive the carbonate system but are not fully represented by the model dynamics. These difficulties stem from the poor representation of the dilution or concentration effects driven by precipitation and evaporation, the accuracy of current atmospheric models, and/or the fact that remote sensing data are insufficient to adequately portray these processes. For the MAB, the simulated air-sea CO_2 flux was controlled by the cross-shelf transport of organic matter (Fennel & Wilkin 2009), the effective TA flux from shelf denitrification (Fennel et al. 2006), and near-surface wind speed (Previdi et al.

2009), all with different space and time variability. More detailed challenges in simulating these complex regimes are provided in **Supplemental Material Section 4**.

In spite of these limitations and challenges, regional and nested coupled physical-biogeochemical models have advanced sufficiently in process representation and skill to allow scenario testing for responses of carbon cycling in coastal waters to past conditions of global and local forcing, as well as projected future conditions. Mathis et al. (2019) used a nested model forced by representative concentration pathway (RCP) climate change scenarios to investigate future reductions in open inflows to the North Sea and showed that this may not necessarily lead to lower biological carbon uptake in the region. Xiu et al. (2018) modeled a complex biological carbon uptake pattern in the California Current System in response to future global warming.

Representative concentration pathway: a trajectory of atmospheric greenhouse gas concentration (not emissions) that describes climate futures

5.3. Challenges for Coupled Circulation-Biogeochemical Models

Simulation of coastal ocean carbon dynamics is dependent on realistic representation of the physical circulation that is governed by both geostrophic (e.g., topographically driven flow) and ageostrophic dynamics (e.g., mixing and nonlinearity), input of terrestrial buoyancy, and water mass and momentum exchanges between the coastal and open oceans (Gan et al. 2010). Accurate representation of the coastal circulation dynamics is challenging because of the temporally variable and spatially heterogeneous processes that link the land and the open ocean. The spatio-temporal resolution required to resolve local topographic controls and high-frequency forcing (such as tides) also introduces challenges for numerical approaches. Another considerable challenge to biogeochemical modeling is the quantification of the parameters that control carbon cycling rates, which are limited by understanding of ecosystem dynamics and observational capabilities.

Simulation of the coastal ocean carbon dynamics also requires three-dimensional boundary fluxes and forcing, some of which can be provided by downscaling of fields from large-scale or global models, which are not always reliable. In addition, numerical open boundary conditions for downscaled fields that allow computational stability and retain the continuum between coastal and open oceans remain an important challenge, although the issue is often neglected (Liu & Gan 2017).

Specification of other boundary fluxes and forcing, such as riverine inputs and ocean nutrient inputs, requires different approaches that depend on climatology and observations (e.g., Fennel et al. 2008), reanalysis products, or other models (Fennel & Wilkin 2009). However, these approaches resolve different spatio-temporal scales and potentially different dynamics (i.e., biogeochemical processes) that may not match those resolved in a regional model. Thus, the current approaches used to specify boundary fluxes and forcing impose constraints and limitations on model skill and simulation results. An important challenge for coastal carbon models is thus to resolve these potential mismatches and not introduce additional uncertainties into simulations.

5.4. State of Current Understanding

Global models offer a large-scale perspective that is useful in informing global assessments of the carbon cycle (e.g., Friedlingstein et al. 2020). However, model constraints imposed by representation of coastal zone circulation dynamics, as well as specific biogeochemical processes relevant to individual regions, have limited the use of GOBMs in studies of coastal carbon cycling. Nevertheless, models with increased resolution have been used for the analysis of long-term trends in coastal carbon without addressing the shorter-term seasonal or interannual temporal variability (Bourgeois et al. 2016, Lacroix et al. 2021a). Analyses of biogeochemical model

structure, complexity, and uncertainty show that increasing model skill is a trade-off between including additional components, accurate representation of rates and processes, and data to constrain processes and provide verification (Ward et al. 2010), all of which have implications for data requirements and process understanding for model parameterization, calibration, and verification.

A limitation of regional and global biogeochemical models is the lack of representation of benthic formation and dissolution of $CaCO_3$, which is an essential component of the carbon counter pump in the coastal ocean (e.g., Smith & Mackenzie 2016). The global role of benthic carbonate cycling has recently been addressed in a conceptual model framework (O'Mara & Dunne 2019), which provides insights into how these processes can be incorporated into three-dimensional coupled physical-biogeochemical models. Representation of organic matter decomposition in the water column and sediments, which generally relies on a limited number of pools or even a single pool of organic matter of constant stoichiometry and reactivity, is another important limitation of global and regional carbon models (Hülse et al. 2018). Also, understanding of how organic matter degrades in marine sediments has implications for development of regional and global carbon models, as well as for elucidation of the role of sediments in carbon budgets (LaRowe et al. 2020). Promising avenues nevertheless exist, such as the representation of terrestrial dissolved organic matter as an independent carbon pool (Lacroix et al. 2021a), or the representation of organic matter degradability across a reactive continuum (Aumont et al. 2017).

Assessment of model skill via comparisons with observations, which often have limitations, or via model intercomparisons is a critical step in refining model structure, determining model-specific responses of biogeochemical cycles to short- (change in land cover) versus long-term (climate) forcing, and developing scenarios to explore the consequences of natural and anthropogenic changes. An important limitation of current models is that model-based estimates are typically not constrained by uncertainty estimates, although efforts have begun to emerge (Meier et al. 2019). In contrast to the open ocean, large-scale carbon models, identifying common, overarching research questions remains very often elusive for coastal carbon models. Therefore, assessing model uncertainties through ensemble runs that address key metrics of the carbon cycle is so far uncommon (Meier et al. 2018). Thus, developing scenarios and overarching questions focused on fundamental controls of the coastal carbon cycle provides an important challenge to the modeling community.

Projecting the consequences of natural and human-induced changes will place more emphasis on models (Jacox et al. 2020). Moreover, coastal ecosystem goods and services will continue to expand (Martínez et al. 2007) as human development leads to more demands (Pendleton et al. 2012), thus further stressing coastal carbon resources. The ability to predict the impacts of multiple stressors and respond to management requirements for coastal resources will require coastal carbon modeling frameworks that can inform economic, social, and governance structures, which remain to be developed.

6. TEMPORAL EVOLUTION OF COASTAL OCEAN CARBON SINK AND ITS POSSIBLE FUTURE TRENDS UNDER POSTIVE AND NEGATIVE EMISSION SCENARIOS

The injection of anthropogenic CO_2 into the atmosphere and its subsequent distribution across the ocean, land, and atmosphere components of the Earth system have led to an unprecedented perturbation of the global carbon cycle that has been ongoing since the Industrial Revolution (Gruber et al. 2019). The ocean, a sustained sink for anthropogenic CO_2 released into the atmosphere by fossil fuel burning over the past ~150 years (**Supplemental Figure 5.1**), has been altered by this CO_2 uptake, and the effects of this perturbation are evident in the coastal ocean.

The complexities of the land-ocean-atmosphere coupled system introduce large uncertainties into projections of ocean carbon fluxes, in particular into defining the role of the coastal carbon sink and its evolution, both of which are of fundamental importance to climate science and climate policies developed before and after achievement of net-zero CO_2 emissions (i.e., carbon neutrality).

Carbon neutrality: a state in which anthropogenic CO_2 emissions are balanced globally by anthropogenic CO_2 removals over a specified period

The Paris Agreement defined climate warming targets of 2°C, 1.5°C, and 1°C, associated with end-of-century atmospheric CO_2 concentrations of ca. 450, 400, and 350 ppm, respectively. These scenarios approach carbon neutrality by about 2070, 2055, and 2040, respectively, and remain negative thereafter (Hansen et al. 2017). More than 130 countries have proposed commitments on the reduction of individual carbon neutrality–related emission.

Adoption and implementation of the actions proposed by many countries will introduce another set of perturbations to the Earth system on decadal timescales. Continued emission growth, followed by the transition from peak to net-zero emissions (2040–2060), will be superimposed on changes that have already occurred throughout the industrial era. Confounding this adjustment to emissions are intended CDR (e.g., artificial ocean alkalinization) and ecosystem restoration (e.g., mangrove forest restoration) activities that are planned or already underway. The combination of these activities will again affect the global carbon cycle by producing abrupt CO_2 redistribution within the Earth system, including at the land-ocean interface. Understanding the response of the coastal ocean carbon sink to these perturbations, individually and collectively, is a major challenge that has implications for the overall global carbon budget and carbon-climate coupled system. The temporal evolution of the air-sea CO_2 flux in the coastal ocean from preindustrial to present time provides useful guidance for suggesting scenarios for possible future trends (**Figure 6**).

6.1. From Preindustrial to Present Time

Analysis of coastal ocean carbon cycling based on conceptual box models suggested that the global continental margin was a preindustrial source of atmospheric CO_2, providing 0.1–0.3 Pg C year^{-1} (intermediate value of ∼0.2 Pg C year^{-1} in **Figure 6*a***) as a result of respiring terrestrially derived organic matter (e.g., Mackenzie & Lerman 2006; Mackenzie et al. 2004, 2002, 2000). Bauer et al. (2013) further suggested that over the past century these ocean margins have progressively shifted to a CO_2 sink of −0.1 to −0.4 Pg C year^{-1} as a result of rising atmospheric CO_2 levels, circulation changes, and increasing riverine nutrient inputs. This source-to-sink shift suggests a current anthropogenic CO_2 sink of −0.2 to −0.7 Pg C year^{-1} (intermediate value of ∼−0.45 Pg C year^{-1} in **Figure 6*b***), with a larger flux density than the open ocean, which is driven by enhanced biological production in the coastal ocean (Mackenzie et al. 2000, 2004).

In contrast, simulations using a GOBM suggested that the preindustrial coastal ocean may have been a CO_2 sink of −0.04 Pg C year^{-1} (Lacroix et al. 2021a), mostly driven by low temperate and biological production on outer shelves and efficient offshore export of terrestrial dissolved organic matter. The same simulations indicated that this sink increased to −0.15 Pg C year^{-1} in present time, suggesting a current anthropogenic CO_2 uptake of only −0.11 Pg C year^{-1} (Lacroix et al. 2020). In another GOBM-based analysis, Bourgeois et al. (2016) found a similar anthropogenic sink of −0.12 Pg C year^{-1}. The lower anthropogenic coastal CO_2 sink suggested by the GOBMs compared to that estimated using box models and mass balance analysis may be a result of different definitions and representations of the coastal ocean. Global box models do not consider the circulation heterogeneity of different coastal regions, which is explicitly resolved in GOBMs, thereby producing shorter water residence time on the shelves (Lacroix et al. 2021a), although the resolution of GOBMs remains too coarse to fully resolve the physical processes on continental shelves. In contrast, box models typically include estuaries, salt marshes, and

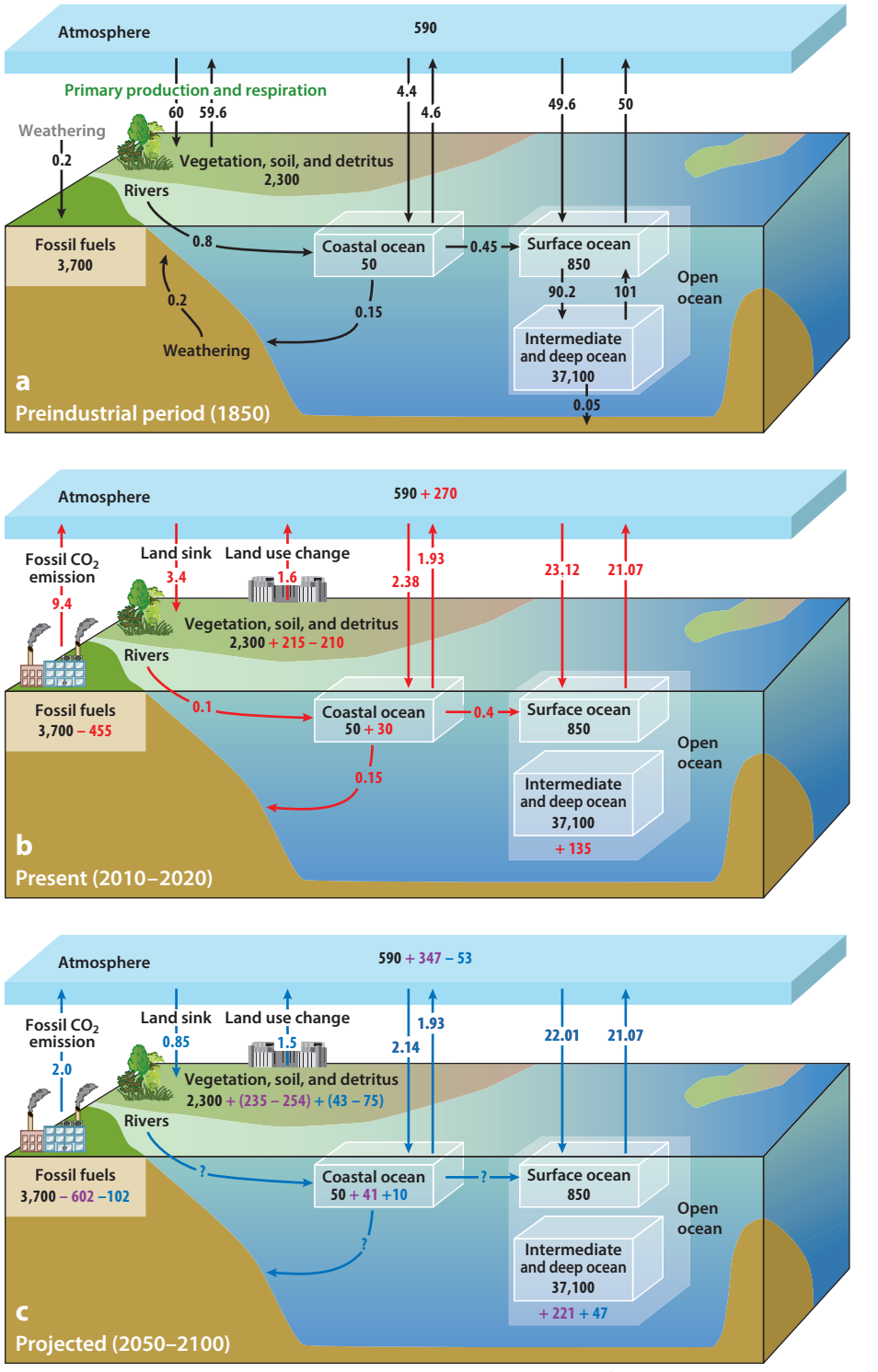

(*Caption appears on following page*)

Figure 6 (*Figure appears on preceding page*)

Schematic of (*a*) preindustrial (1850), (*b*) present (2010–2020), and (*c*) future (2050–2100) global carbon budgets. Fluxes of total carbon (organic plus inorganic, in Petagrams of carbon per year) between different reservoirs (numbers in the boxes represent the reservoirs in Petagrams of carbon) for preindustrial (*black arrows* and *numbers*; natural background), present (*red arrows* and *numbers*; anthropogenically induced changes), and after carbon neutrality (*blue arrows* and *numbers*; anthropogenically induced changes) are estimated based on Sarmiento & Gruber (2002), Aricò et al. (2021), Bauer et al. (2013), Friedlingstein et al. (2020), Regnier et al. (2013b), and Jones et al. (2016). The fluxes in panels *b* and *c* are on top of the natural fluxes in panel *a*. In panel a, the land source of 59.6 Pg C $year^{-1}$ includes the degassing of ∼1 Pg C $year^{-1}$ from inland waters during the preindustrial era. The cumulative CO_2 from 1850 to 2050 when the cumulative CO_2 in the atmosphere is expected to peak (Jones et al. 2016) is shown in panel *c* (*purple numbers*). For the land sink, the positive number is an inferred terrestrial land sink and the negative value is the decrease due to deforestation. In panels *a* and *b*, the gross oceanic carbon source to the atmosphere is partitioned between the coastal ocean and the open ocean based on surface area proportions of 8.4% for the global coastal ocean and 91.6% for the open ocean. In panels *b* and *c*, the increase in the coastal ocean carbon inventory is estimated based on the ratio of contemporary anthropogenic CO_2 uptake by the coastal ocean to global ocean. Details of the estimates are provided in **Supplemental Material Section 6**.

mangroves, the water components of which generally serve as a source of carbon to the atmosphere and are not resolved in three-dimensional GOBMs.

Nevertheless, observational studies have suggested a tendency for enhanced ocean margin uptake of atmospheric CO_2 over the past three decades (Laruelle et al. 2018). Using a conceptual model, Bauer et al. (2013) and Cai (2011) also suggested an increasing global shelf CO_2 sink in response to increased atmospheric pCO_2. These observation- and model-based studies agree that temperate and subpolar shelves may be stronger sinks of anthropogenic CO_2 than the open ocean. In contrast, modeling studies suggest weak anthropogenic sinks for most tropical and Arctic shelves, regions that are poorly represented in the study of Laruelle et al. (2018), and may explain the differing conclusions at the global scale.

Significant differences in trends of air-sea CO_2 fluxes, however, occur between many coastal regions and the adjacent open-ocean waters, particularly for coastal upwelling systems (e.g., Peruvian upwelling current, OceMar) and those dominated by large river plumes (e.g., Amazon River plume, RiOMar) (Bourgeois et al. 2016). The three case studies presented in Section 4 also demonstrated clear differences in long-term trends of CO_2 fluxes. These observed differences indicate that physical and/or biogeochemical processes other than the abiotic atmospheric CO_2 can be important controls on carbon flux evolution in specific coastal regions.

The different models are consistent in identifying terrestrial inputs via river discharges and ocean margin-open ocean exchanges as primary controls of coastal ocean carbon cycling. Regnier et al. (2013b) suggested an anthropogenic perturbation of an enhanced riverine discharge flux of 0.10 Pg C $year^{-1}$ (**Figure 6*b***), 70% of which can be exported to the open ocean (Bourgeois et al. 2016). Increased riverine nutrients and TA loads affect coastal carbon cycling by enhanced biological uptake and changes in seawater buffering capacity, which are rarely represented in current GOBMs that assume constant present-day riverine loads of both carbon and nutrients. Lacroix et al. (2020) estimated that present-day global riverine nutrients loads have increased relative to preindustrial times by 8–197%, 37–144%, and 115–141% for phosphorus, nitrogen, and silicate, respectively (Beusen et al. 2009, 2016; Frings et al. 2016; Mayorga et al. 2010). Changes in TA are less well constrained, although Goll et al. (2014) suggested an increase of ca. 11% in the weathering supply of alkalinity over the historical time period. A schematic for the evolution of the land-derived forcing is shown in **Supplemental Figure 5.2**.

With increased terrestrial inputs into the coastal ocean, the anthropogenic-induced increase in sedimentary burial of organic carbon and the lateral export to the open ocean are estimated to

be 0.15 (Regnier et al. 2013b) and 0.4 Pg C year^{-1} (Bauer et al. 2013), respectively, comparable to the natural fluxes at preindustrial times (**Figure 6*a*,*b***). The enhanced biological production and carbon sink increased the coastal ocean carbon inventory by 30 Pg C from 1850 to 2010–2020, nearly 60% of the coastal ocean carbon inventory estimated for preindustrial times.

RCP 2.6: one pathway where radiative forcing peaks at approximately 3 W m^{-2} and then declines to be limited at 2.6 W m^{-2} in 2100

6.2. From Present to Future

The temporal evolution of atmospheric pCO_2 at the end of this century has been assessed for various RCP scenarios. Under the low carbon or neutrality scenario (RCP 2.6), atmospheric CO_2 will peak in two to three decades followed by a gradual decrease until the end of this century (**Supplemental Figure 5.2*i***). In response to these projected atmospheric CO_2 changes, the strength of the global ocean carbon sink may slowly increase for another 10 years but rapidly shift to a continuous decrease (Jones et al. 2016). The eventual decline in atmospheric pCO_2 under the RCP 2.6 scenario may be offset by CO_2 fluxes from the ocean, an expected ocean feedback to reductions in emissions (Keller et al. 2018, Koch et al. 2021). Implementation of marine CDR would be needed to sustain the ocean carbon sink, which may further change ocean carbon cycling.

With progressive emission reductions and CDR, the atmospheric pCO_2 will decline and eventually approximate that of sea surface water, resulting in a less efficient natural uptake of atmospheric CO_2 in the coastal ocean (**Supplemental Figure 5.2*k***). Changes in coastal-ocean physics and biology as well as in riverine inputs and sediment interactions will modify the distribution of carbon and alkalinity (Hu & Cai 2011, Mackenzie et al. 2004), also affecting the potential of the coastal ocean to absorb anthropogenic carbon. A potential future outcome is that enhanced anthropogenic activities (Regnier et al. 2013b) and precipitation (Battin et al. 2009) will increase carbon export from land to the coastal ocean. Riverine organic carbon inputs tend to produce excess DIC in the coastal ocean because of efficient remineralization of the higher carbon to nitrogen ratio in terrestrial organic matter relative to use by aquatic primary production (Bauer et al. 2013, Lacroix et al. 2020). Another possibility is a decline in the terrestrial input of nutrients after the peak of fertilizer use (**Supplemental Figure 5.2*c*,*d***), producing reduced DIC deficits in RiOMar systems and leading to a decline in coastal ocean carbon sinks and carbon burial (**Supplemental Figure 5.2**).

The responses of OceMar systems are complex because of the influence of boundary currents that are part of the large-scale ocean basin circulation (**Supplemental Figure 5.2*g*–*i***). Taking the ocean margins adjacent to the WBC in the WNP as an example, warming in the Kuroshio region would lead to a northward shift of the subtropical circulation system (Hu et al. 2015) and strengthening of the Kuroshio (Chen et al. 2015), thereby weakening the intrusion of open ocean water masses into the adjacent ocean margins (e.g., Wu et al. 2017). As a result, reduced nutrient and DIC influxes from the open ocean would be expected. Projections for EBC systems suggest that the strength of these upwelling systems will be enhanced under warming scenarios (Sydeman et al. 2014), thereby increasing the supply of carbon and nutrients from depth to the surface waters. However, how the CO_2 source/sink role of OceMar systems will change is dependent on changes in the ratio between DIC and nutrients of source waters and the physical settings that affect water residence times and hence biological controls on the carbon cycle.

Interventions that move toward carbon neutrality will significantly influence the global carbon cycle and the carbon fluxes among different reservoirs. Anthropogenic carbon emissions are projected to decrease by more than two-thirds between 2050 and 2100 under the RCP 2.6 scenario, reducing the atmospheric carbon inventory by 53 Pg C (**Figure 6*c***). Correspondingly, the carbon sink of the ocean, either the open or coastal ocean, will also decrease by more than half relative to the present-day scenario, from −2.05 to −0.94 Pg C year^{-1} for the open ocean

and from −0.45 to −0.21 Pg C $year^{-1}$ for the coastal ocean (**Figure 6*b*,*c***). The carbon inventory of the coastal ocean and open ocean is estimated to increase by 10 and 47 Pg C, respectively, relative to the present-day scenario (**Figure 6*c***). The coastal ocean carbon budget thus shows the greatest response to progressive future reductions in emission reductions and implementation of CDR techniques. However, carbon transport fluxes along the land-coastal ocean-open ocean continuum under low carbon emission scenarios are essentially unknown (**Figure 6*c***). Thus, the challenges associated with identifying and quantifying current and projected responses of the coastal ocean and its source/sink role in the global carbon budget are daunting. Addressing these challenges requires coordinated observational and modeling efforts focused at both regional and global scales. The development of these programs is a priority for the ocean carbon research and management community.

SUMMARY POINTS

1. Rapid increases in ocean carbon observations have allowed further improvement in estimating the global coastal ocean CO_2 sink and its spatial distribution. An updated compilation of air-sea CO_2 fluxes based on observations reported in the literature shows that the global coastal ocean represents an integrated CO_2 sink of -0.25 ± 0.05 Pg C $year^{-1}$ with a flux density of -0.68 ± 0.14 mol C m^{-2} $year^{-1}$, confirming that the coastal ocean is an efficient CO_2 sink. The strongest CO_2 uptake occurs at high latitudes with the combined contributions from polar (−134 Tg C $year^{-1}$) and subpolar (−108 Tg C $year^{-1}$) regions accounting for the majority of the global coastal carbon sink. Moderate CO_2 uptake with highest seasonal dynamic ranges occurs at mid-latitudes. Alternating uptake and outgassing of CO_2 occurs at low latitudes. The latitudinal pattern in CO_2 flux and its seasonality are controlled by both temperature and nonthermal factors, such as water mass mixing and net primary production, characteristics of coastal ocean carbon cycling that differ from those of the open ocean.
2. A framework based on river-dominated ocean margin (RiOMar) and ocean-dominated margin (OceMar) systems is used to conceptualize coastal ocean carbon cycle processes and provide a semiquantitative diagnosis of individual coastal ocean systems. Application of this framework highlights differences in exchanges and boundary transport along the river-estuary-shelf-ocean continuum and the intrinsic biogeochemical reactions that determine air-sea CO_2 fluxes.
3. Coastal ocean carbon models, extending from conceptual box (budget) models to three-dimensional coupled circulation-biogeochemical models, have been successfully implemented in a range of coastal ocean regions. These models simulate key processes, provide projections of future trends, and highlight uncertainties and challenges in our understanding of coastal carbon cycling. Global ocean biogeochemical models (GOBMs) with improved spatial resolution allow simulation of important features and global trends in the global coastal ocean, such as coastal water residence times, air-sea CO_2 exchange, and riverine fluxes. GOBMs are also instrumental in simulating global trends in coastal carbon cycle processes and fluxes.
4. Observations and numerical model simulations are revealing long-term trends in ocean carbon fluxes, which have been perturbed since preindustrial times. The anthropogenic alterations are anticipated to continue before and after net-zero CO_2 emissions (i.e.,

carbon neutrality) are reached, but considerable uncertainty is associated with impacts arising from concurrent changes in the land-ocean-atmosphere coupled system. The observed differences in carbon fluxes and their long-term trends among different coastal systems indicate that physical and/or biogeochemical processes other than the abiotic atmospheric CO_2 can be important controls on the evolution of air-sea CO_2 exchanges in specific coastal regions.

FUTURE ISSUES

1. The ability to conceptualize and simulate future trends in the coastal ocean carbon cycle has been greatly advanced by improved understanding of spatio-temporal variability of carbon fluxes. This highlights the importance of continuing and enhancing ocean carbon observation programs that are coordinated with measurements of physical, chemical, and biological parameters that can be used to provide information that is responsive to regional interests, policies, and management. The continued development of global data products, such as the Surface Ocean CO_2 Atlas, with improved coordination across the land-ocean continuum is critical to further advance understanding of ocean carbon dynamics.
2. Regional models that fully couple the land-ocean continuum and global coastal ocean models that meaningfully resolve and reconcile coastal physical processes are equally important for the development of predictive capabilities at both regional and global scales. Predictive capability is increasingly needed to project the role of the coastal ocean in the global carbon cycle and inform policies developed to achieve net-zero carbon emissions by the mid-twenty-first century. Here, improvements in data collection and advances in model structure and computational resources that allow integration of data and models are essential priorities. Improved representation of coastal processes through use of conceptual frameworks such as the RiOMar and OceMar systems provides an avenue to improve model skill and identify needed observations.
3. Identification of a baseline conditions representative of preindustrial times is critical for assessing past effects of human activities and for projecting future trends in coastal ocean carbon cycling and air-sea CO_2 fluxes. Estimating this baseline condition and its associated uncertainty has important implications for advancing the ability to detect and quantify changes in the coastal ocean carbon cycle.

DISCLOSURE STATEMENT

The authors are not aware of any affiliations, memberships, funding, or financial holdings that might be perceived as affecting the objectivity of this review.

ACKNOWLEDGMENTS

We would like to thank Xianghui Guo, Yuye Han, Yaohua Luo, Yanping Xu, Yan Yang, Wei Yang, Yan Bai, Shujie Yu, Zigeng Song, and Kuanbo Zhou for their support and help in preparing the data, figures, and references used in this contribution. We acknowledge Alizée Roobaert

and Shuping Zhang for providing latitudinal distributions of annual CO_2 fluxes and surface pCO_2 climatology data for the Baltic Sea. This study is a contribution to the Regional Carbon Cycle Assessment and Processes Phase 2 supported by the Global Carbon Project. The Surface Ocean CO_2 Atlas (SOCAT) is an international effort, endorsed by the International Ocean Carbon Coordination Project (IOCCP), the Surface Ocean Lower Atmosphere Study (SOLAS), and the Integrated Marine Biosphere Research (IMBeR) program to deliver a uniformly quality-controlled surface ocean CO_2 database. The many researchers and funding agencies responsible for the collection of data and quality control are thanked for their contributions to SOCAT. Support for M.D. was provided by National Natural Science Foundation of China grant 42188102. Support for E.E.H. was provided by National Oceanic and Atmospheric Administration (NOAA) grant NA16NOS4780207. W.-J.C. acknowledges support by the National Science Foundation and NOAA. P.A.G.R. received financial support from Belgian Science Policy Office through the project ReCAP, which is part of the Belgian research program FedTwin, and from the European Union's Horizon 2020 research and innovation program under grant agreements 776810 (VERIFY) and 101003536 (ESM2025–Earth System Models for the Future).

LITERATURE CITED

Abrahamsen EP, Meredith MP, Falkner KK, Torres-Valdes S, Leng MJ, et al. 2009. Tracer-derived freshwater composition of the Siberian continental shelf and slope following the extreme Arctic summer of 2007. *Geophys. Res. Lett.* 36:L07602

Aiello IW, Ravelo AC. 2012. Evolution of marine sedimentation in the Bering Sea since the Pliocene. *Geosphere* 8:1231–53

Aricò S, Arrieta JM, Bakker DCE, Boyd PW, Cotrim da Cunha L, et al. 2021. *Integrated Ocean Carbon Research: A Summary of Ocean Carbon Research, and Vision of Coordinated Ocean Carbon Research and Observations for the Next Decade*. Paris: UNESCO-IOC

Aumont O, van Hulten M, Roy-Barman M, Dutay JC, Éthé C, Gehlen M. 2017. Variable reactivity of particulate organic matter in a global ocean biogeochemical model. *Biogeosciences* 14:2321–41

Bakker DCE, Pfeil B, Landa CS, Metzl N, O'Brien KM, et al. 2016. A multi-decade record of high-quality fCO_2 data in version 3 of the Surface Ocean CO_2 Atlas (SOCAT). *Earth Syst. Sci. Data* 8:383–413

Bates NR, Mathis JT, Jeffries MA. 2011. Air-sea CO_2 fluxes on the Bering Sea shelf. *Biogeosciences* 8:1237–53

Battin TJ, Luyssaert S, Kaplan LA, Aufdenkampe AK, Richter A, Tranvik LJ. 2009. The boundless carbon cycle. *Nat. Geosci.* 2:598–600

Bauer JE, Cai WJ, Raymond PA, Bianchi TS, Hopkinson CS, Regnier PAG. 2013. The changing carbon cycle of the coastal ocean. *Nature* 504:61–70

Beszczynska-Möller A, Fahrbach E, Schauer U, Hansen E. 2012. Variability in Atlantic water temperature and transport at the entrance to the Arctic Ocean, 1997–2010. *ICES J. Mar. Sci.* 69:852–63

Beusen AHW, Bouwman AF, Durr HH, Dekkers ALM, Hartmann J. 2009. Global patterns of dissolved silica export to the coastal zone: results from a spatially explicit global model. *Glob. Biogeochem. Cycles* 23:GB0A02

Beusen AHW, Bouwman AF, Van Beek LPH, Mogollon JM, Middelburg JJ. 2016. Global riverine N and P transport to ocean increased during the 20th century despite increased retention along the aquatic continuum. *Biogeosciences* 13:2441–51

Bianchi TS, Aller RC, Atwood TB, Brown CJ, Buatois LA, et al. 2021. What global biogeochemical consequences will marine animal–sediment interactions have during climate change? *Elem. Sci. Anthropocene* 9:00180

Borges AV. 2005. Do we have enough pieces of the jigsaw to integrate CO_2 fluxes in the coastal ocean? *Estuaries* 28:3–27

Borges AV, Delille B, Frankignoulle M. 2005. Budgeting sinks and sources of CO_2 in the coastal ocean: diversity of ecosystems counts. *Geophys. Res. Lett.* 32:L14601

Bourgeois T, Orr JC, Resplandy L, Terhaar J, Ethé C, et al. 2016. Coastal-ocean uptake of anthropogenic carbon. *Biogeosciences* 13:4167–85

Brand TD, Griffiths C. 2009. Seasonality in the hydrography and biogeochemistry across the Pakistan margin of the NE Arabian Sea. *Deep-Sea Res. II* 56:283–95

Cai W-J. 2011. Estuarine and coastal ocean carbon paradox: CO_2 sinks or sites of terrestrial carbon incineration? *Annu. Rev. Mar. Sci.* 3:123–45

Cai W-J, Chen CTA, Borges A. 2014. Carbon dioxide dynamics and fluxes in coastal waters influenced by river plumes. In *Biogeochemcial Dynamics at Major River-Coastal Interfaces—Linkages with Global Change*, ed. TS Bianchi, MA Allison, W-J Cai, pp. 155–73. New York: Cambridge Univ. Press

Cai W-J, Dai M, Wang Y. 2006. Air-sea exchange of carbon dioxide in ocean margins: a province-based synthesis. *Geophys. Res. Lett.* 33:L12603

Cai W-J, Dai MH. 2004. Comment on "Enhanced open ocean storage of CO_2 from shelf sea pumping." *Science* 306:1477

Cai W-J, Xu YY, Feely RA, Wanninkhof R, Jonsson B, et al. 2020. Controls on surface water carbonate chemistry along North American ocean margins. *Nat. Commun.* 11:2691

Cao ZM, Dai MH, Evans W, Gan JP, Feely R. 2014. Diagnosing CO_2 fluxes in the upwelling system off the Oregon–California coast. *Biogeosciences* 11:6341–54

Cao ZM, Yang W, Zhao YY, Guo XH, Yin ZQ, et al. 2020. Diagnosis of CO_2 dynamics and fluxes in global coastal oceans. *Natl. Sci. Rev.* 7:786–97

Chen C-TA. 1985. Preliminary observations of oxygen and carbon dioxide of the wintertime Bering Sea marginal ice zone. *Cont. Shelf Res.* 4:465–83

Chen C-TA, Andreev A, Kim K-R, Yamamoto M. 2004. Roles of continental shelves and marginal seas in the biogeochemical cycles of the North Pacific Ocean. *J. Oceanogr.* 60:17–44

Chen C-TA, Borges AV. 2009. Reconciling opposing views on carbon cycling in the coastal ocean: continental shelves as sinks and near-shore ecosystems as sources of atmospheric CO_2. *Deep-Sea Res. II* 56:578–90

Chen C-TA, Huang TH, Chen YC, Bai Y, He X, Kang Y. 2013. Air–sea exchanges of CO_2 in the world's coastal seas. *Biogeosciences* 10:6509–44

Chen C-TA, Wang S-L. 1999. Carbon, alkalinity and nutrient budgets on the East China Sea continental shelf. *J. Geophys. Res.* 104(C9):20675–86

Chen X, Qiu B, Chen S, Qi Y, Du Y. 2015. Seasonal eddy kinetic energy modulations along the North Equatorial Countercurrent in the western Pacific. *J. Geophys. Res. Oceans* 120:6351–62

Chou WC, Tishchenko PY, Chuang KY, Gong GC, Shkirnikova EM, Tishchenko PP. 2017. The contrasting behaviors of CO_2 systems in river-dominated and ocean-dominated continental shelves: a case study in the East China Sea and the Peter the Great Bay of the Japan/East Sea in summer 2014. *Mar. Chem.* 195:50–60

Ciais P, Sabine C, Bala G, Bopp L, Brovkin V, et al. 2013. Carbon and other biogeochemical cycles. In *Climate Change 2013: The Physical Science Basis*, ed. TF Stocker, D Qin, G-K Plattner, M Tignor, SK Allen, et al., pp. 465–570. New York: Cambridge Univ. Press

Cooley SR, Kite-Powell HL, Doney SC. 2009. Ocean acidification's potential to alter global marine ecosystem services. *Oceanography* 22:172–81

Cross JN, Mathis JT, Frey KE, Cosca CE, Danielson SL, et al. 2014. Annual sea-air CO_2 fluxes in the Bering Sea: insights from new autumn and winter observations of a seasonally ice-covered continental shelf. *J. Geophys. Res. Oceans* 119:6693–708

Dai MH. 2021. What are the exchanges of carbon between the land-ocean-ice continuum? In *Integrated Ocean Carbon Research: A Summary of Ocean Carbon Research, and Vision of Coordinated Ocean Carbon Research and Observations for the Next Decade*, ed. R Wanninkhof, C Sabine, S Aricò, p. 14. Paris: UNESCO-IOC

Dai MH, Cao ZM, Guo XH, Zhai WD, Liu ZY, et al. 2013. Why are some marginal seas sources of atmospheric CO_2? *Geophys. Res. Lett.* 40:2154–58

DeGrandpre MD, Olbu GJ, Beatty CM, Hammar TR. 2002. Air–sea CO_2 fluxes on the US Middle Atlantic Bight. *Deep-Sea Res. II* 49:4355–67

Druon JN, Mannino A, Signorini S, McClain C, Friedrichs M, et al. 2010. Modeling the dynamics and export of dissolved organic matter in the Northeastern US continental shelf. *Estuar. Coast. Shelf Sci.* 88:488–507

Dunne JP, Winton M, Bacmeister J, Danabasoglu G, Gettelman A, et al. 2020. Comparison of equilibrium climate sensitivity estimates from slab ocean, 150-year, and longer simulations. *Geophys. Res. Lett.* 47:e2020GL088852

Feely RA, Sabine CL, Hernandez-Ayon JM, Ianson D, Hales B. 2008. Evidence for upwelling of corrosive "acidified" water onto the continental shelf. *Science* 320:1490–92

Fennel K, Testa JM. 2019. Biogeochemical controls on coastal hypoxia. *Annu. Rev. Mar. Sci.* 11:105–30

Fennel K, Wilkin J. 2009. Quantifying biological carbon export for the northwest North Atlantic continental shelves. *Geophys. Res. Lett.* 36:L18605

Fennel K, Wilkin J, Levin J, Moisan J, O'Reilly J, Haidvogel D. 2006. Nitrogen cycling in the Middle Atlantic Bight: results from a three-dimensional model and implications for the North Atlantic nitrogen budget. *Glob. Biogeochem. Cycles* 20:GB3007

Fennel K, Wilkin J, Previdi M, Najjar R. 2008. Denitrification effects on air-sea CO_2 flux in the coastal ocean: simulations for the northwest North Atlantic. *Geophys. Res. Lett.* 35:L24608

Fransner F, Gustafsson E, Tedesco L, Vichi M, Hordoir R, et al. 2018. Non-Redfieldian dynamics explain seasonal pCO_2 drawdown in the Gulf of Bothnia. *J. Geophys. Res. Oceans* 123:166–88

Friedlingstein P, O'Sullivan M, Jones MW, Andrew RM, Hauck J, et al. 2020. Global carbon budget 2020. *Earth Syst. Sci. Data* 12:3269–340

Frings PJ, Clymans W, Fontorbe G, De La Rocha CL, Conley DJ. 2016. The continental Si cycle and its impact on the ocean Si isotope budget. *Chem. Geol.* 425:12–36

Frischknecht M, Munnich M, Gruber N. 2018. Origin, transformation, and fate: the three-dimensional biological pump in the California Current System. *J. Geophys. Res. Oceans* 123:7939–62

Gallegos A. 1996. Descriptive physical oceanography of the Caribbean Sea. In *Small Islands: Marine Science and Sustainable Development*, ed. GA Maul, pp. 36–55. Washington, DC: Am. Geophys. Union

Gan J, Qu T. 2008. Coastal jet separation and associated flow variability in the southwest South China Sea. *Deep-Sea Res. I* 55:1–19

Gan JP, Li L, Wang DX, Guo XG. 2009. Interaction of a river plume with coastal upwelling in the northeastern South China Sea. *Cont. Shelf Res.* 29:728–40

Gan JP, Lu ZM, Dai MH, Cheung AYY, Liu HB, Harrison P. 2010. Biological response to intensified upwelling and to a river plume in the northeastern South China Sea: a modeling study. *J. Geophys. Res.* 115(C9):C09001

Gattuso JP, Frankignoulle M, Wollast R. 1998. Carbon and carbonate metabolism in coastal aquatic ecosystems. *Annu. Rev. Ecol. Syst.* 29:405–34

Goll DS, Moosdorf N, Hartmann J, Brovkin V. 2014. Climate-driven changes in chemical weathering and associated phosphorus release since 1850: implications for the land carbon balance. *Geophys. Res. Lett.* 41:3553–58

Gomez FA, Wanninkhof R, Barbero L, Lee SK, Hernandez FJ Jr. 2020. Seasonal patterns of surface inorganic carbon system variables in the Gulf of Mexico inferred from a regional high-resolution ocean biogeochemical model. *Biogeosciences* 17:1685–700

Grosse J, Bombar D, Doan HN, Nguyen LN, Voss M. 2010. The Mekong River plume fuels nitrogen fixation and determines phytoplankton species distribution in the South China Sea during low and high discharge season. *Limnol. Oceanogr.* 55:1668–80

Gruber N, Clement D, Carter BR, Feely RA, van Heuven S, et al. 2019. The oceanic sink for anthropogenic CO_2 from 1994 to 2007. *Science* 363:1193–99

Guo XH, Zhai WD, Dai MH, Zhang C, Bai Y, et al. 2015. Air-sea CO_2 fluxes in the East China Sea based on multiple-year underway observations. *Biogeosciences* 12:5495–514

Gustafsson E, Omstedt A, Gustafsson BG. 2015. The air-water CO_2 exchange of a coastal sea—a sensitivity study on factors that influence the absorption and outgassing of CO_2 in the Baltic Sea. *J. Geophys. Res. Oceans* 120:5342–57

Hansen B, Østerhus S, Turrell WR, Jónsson S, Valdimarsson H, et al. 2008. The inflow of Atlantic water, heat, and salt to the Nordic Seas across the Greenland–Scotland Ridge. In *Arctic–Subarctic Ocean Fluxes: Defining the Role of the Northern Seas in Climate*, ed. RR Dickson, J Meincke, P Rhines, pp. 15–43. Dordrecht, Neth.: Springer

Hansen J, Sato M, Kharecha P, von Schuckmann K, Beerling DJ, et al. 2017. Young people's burden: requirement of negative CO_2 emissions. *Earth Syst. Dyn.* 8:577–616

Herrmann M, Najjar RG, Kemp WM, Alexander RB, Boyer EW, et al. 2015. Net ecosystem production and organic carbon balance of U.S. East Coast estuaries: a synthesis approach. *Glob. Biogeochem. Cycles* 29:96–111

Hoegh-Guldberg O, Northrop E, Lubchenco J. 2019. The ocean is key to achieving climate and societal goals. *Science* 365:1372–74

Hofmann EE, Cahill B, Fennel K, Friedrichs MAM, Hyde K, et al. 2011. Modeling the dynamics of continental shelf carbon. *Annu. Rev. Mar. Sci.* 3:93–122

Holt J, Wakelin S, Huthnance J. 2009. Down-welling circulation of the northwest European Continental Shelf: a driving mechanism for the continental shelf carbon pump. *Geophys. Res. Lett.* 36:L14602

Hu D, Wu L, Cai W, Gupta AS, Ganachaud A, et al. 2015. Pacific western boundary currents and their roles in climate. *Nature* 522:299–308

Hu X, Cai W-J. 2011. An assessment of ocean margin anaerobic processes on oceanic alkalinity budget. *Glob. Biogeochem. Cycles* 25:GB3003

Huang WJ, Cai WJ, Wang YC, Lohrenz SE, Murrell MC. 2015. The carbon dioxide system on the Mississippi River-dominated continental shelf in the northern Gulf of Mexico: 1. Distribution and air-sea CO_2 flux. *J. Geophys. Res. Oceans* 120:1429–45

Hülse D, Arndt S, Daines S, Regnier P, Ridgwell A. 2018. OMEN-SED 1.0: a novel, numerically efficient organic matter sediment diagenesis module for coupling to Earth system models. *Geosci. Model Dev.* 11:2649–89

Ibanhez JSP, Araujo M, Lefevre N. 2016. The overlooked tropical oceanic CO_2 sink. *Geophys. Res. Lett.* 43:3804–12

Ingvaldsen R, Loeng H, Asplin L. 2002. Variability in the Atlantic inflow to the Barents Sea based on a one-year time series from moored current meters. *Cont. Shelf Res.* 22:505–19

Jacox MG, Alexander MA, Siedlecki S, Chen K, Kwon YO, et al. 2020. Seasonal-to-interannual prediction of North American coastal marine ecosystems: forecast methods, mechanisms of predictability, and priority developments. *Prog. Oceanogr.* 183:102307

Jones CD, Ciais P, Davis SJ, Friedlingstein P, Gasser T, et al. 2016. Simulating the Earth system response to negative emissions. *Environ. Res. Lett.* 11:095012

Kang Y, Pan D, Bai Y, He X, Chen X, et al. 2013. Areas of the global major river plumes. *Acta Oceanol. Sin.* 32:79–88

Keeling CD, Piper SC, Bacastow RB, Wahlen M, Whorf TP, et al. 2005. Atmospheric CO_2 and $^{13}CO_2$ exchange with the terrestrial biosphere and oceans from 1978 to 2000: observations and carbon cycle implications. In *History of Atmospheric CO_2 and Its Effects on Plants, Animals, and Ecosystems*, ed. JR Ehleringer, TE Cerling, MD Dearing, pp. 83–113. New York: Springer

Keller DP, Lenton A, Littleton EW, Oschlies A, Scott V, Vaughan NE. 2018. The effects of carbon dioxide removal on the carbon cycle. *Curr. Clim. Change Rep.* 4:250–65

Kelley JJ, Hood DW. 1971. Carbon dioxide in the surface water of the ice-covered Bering Sea. *Nature* 229:37–39

Koch A, Brierley C, Lewis SL. 2021. Effects of Earth system feedbacks on the potential mitigation of large-scale tropical forest restoration. *Biogeosciences* 18:2627–47

Krumins V, Gehlen M, Arndt S, Van Cappellen P, Regnier P. 2013. Dissolved inorganic carbon and alkalinity fluxes from coastal marine sediments: model estimates for different shelf environments and sensitivity to global change. *Biogeosciences* 10:371–98

Lacroix F, Ilyina T, Hartmann J. 2020. Oceanic CO_2 outgassing and biological production hotspots induced by pre-industrial river loads of nutrients and carbon in a global modeling approach. *Biogeosciences* 17:55–88

Lacroix F, Ilyina T, Laruelle GG, Regnier P. 2021a. Reconstructing the preindustrial coastal carbon cycle through a global ocean circulation model: Was the global continental shelf already both autotrophic and a CO_2 sink? *Glob. Biogeochem. Cycles* 35:e2020GB006603

Lacroix F, Ilyina T, Mathis M, Laruelle GG, Regnier P. 2021b. Historical increases in land-derived nutrient inputs may alleviate effects of a changing physical climate on the oceanic carbon cycle. *Glob. Change Biol.* 27:5491–513

LaRowe DE, Arndt S, Bradley JA, Burwicz E, Dale AW, Amend JP. 2020. Organic carbon and microbial activity in marine sediments on a global scale throughout the Quaternary. *Geochim. Cosmochim. Acta* 286:227–47

Laruelle GG, Cai W-J, Hu X, Gruber N, Mackenzie FT, Regnier P. 2018. Continental shelves as a variable but increasing global sink for atmospheric carbon dioxide. *Nat. Commun.* 9:454

Laruelle GG, Dürr HH, Lauerwald R, Hartmann J, Slomp CP, et al. 2013. Global multi-scale segmentation of continental and coastal waters from the watersheds to the continental margins. *Hydrol. Earth Syst. Sci.* 17:2029–51

Laruelle GG, Dürr HH, Slomp CP, Borges AV. 2010. Evaluation of sinks and sources of CO_2 in the global coastal ocean using a spatially-explicit typology of estuaries and continental shelves. *Geophys. Res. Lett.* 37:L15607

Laruelle GG, Goossens N, Arndt S, Cai WJ, Regnier P. 2017. Air–water CO_2 evasion from US East Coast estuaries. *Biogeosciences* 14:2441–68

Laruelle GG, Lauerwald R, Pfeil B, Regnier P. 2014. Regionalized global budget of the CO_2 exchange at the air-water interface in continental shelf seas. *Glob. Biogeochem. Cycles* 28:1199–214

Legge O, Johnson M, Hicks N, Jickells T, Diesing M, et al. 2020. Carbon on the northwest European shelf: contemporary budget and future influences. *Front. Mar. Sci.* 7:143

Lehrter JC, Ko DS, Murrell MC, Hagy JD, Schaeffer BA, et al. 2013. Nutrient distributions, transports, and budgets on the inner margin of a river-dominated continental shelf. *J. Geophys. Res. Oceans* 118:4822–38

Li D, Gan J, Hui R, Liu Z, Yu L, et al. 2020a. Vortex and biogeochemical dynamics for the hypoxia formation within the coastal transition zone off the Pearl River Estuary. *J. Geophys. Res. Oceans* 125:e2020JC016178

Li Q, Guo X, Zhai W, Xu Y, Dai M. 2020b. Partial pressure of CO_2 and air-sea CO_2 fluxes in the South China Sea: synthesis of an 18-year dataset. *Prog. Oceanogr.* 182:102272

Liu KK, Atkinson L, Quiñones RA, Talaue-McManus L. 2010. Biogeochemistry of continental margins in a global context. In *Carbon and Nutrient Fluxes in Continental Margins*, ed. KK Liu, L Atkinson, R Quiñones, L Talaue-McManus, pp. 3–24. Berlin: Springer

Liu Z, Gan J. 2012. Variability of the Kuroshio in the East China Sea derived from satellite altimetry data. *Deep-Sea Res. I* 59:25–36

Liu Z, Gan J. 2017. Three-dimensional pathways of water masses in the South China Sea: a modeling study. *J. Geophys. Res. Oceans* 122:6039–54

Lohrenz SE, Cai WJ, Chakraborty S, Gundersen K, Murrell MC. 2013. Nutrient and carbon dynamics in a large river-dominated coastal ecosystem: the Mississippi-Atchafalaya River system. In *Biogeochemical Dynamics at Major River-Coastal Interfaces: Linkages with Global Change*, ed. MA Allison, TS Bianchi, W-J Cai, pp. 448–72. Cambridge, UK: Cambridge Univ. Press

MacCready P, Johns WE, Rooth CG, Fratantoni DM, Watlington RA. 1999. Overflow into the deep Caribbean: effects of plume variability. *J. Geophys. Res.* 104(C11):25913–35

Mackenzie FT, Andersson AJ, Lerman A, Ver LM. 2005. Boundary exchanges in the global coastal margin: implications for the organic and inorganic carbon cycles. In *The Sea: The Global Coastal Ocean: Multiscale Interdisciplinary Processes*, ed. AR Robinson, KH Brink, pp. 193–225. Cambridge, MA: Harvard Univ. Press

Mackenzie FT, Lerman A. 2006. Brief Overview of Carbon on Earth. In *Carbon in the Geobiosphere—Earth's Outer Shell*, pp. 1–22. Dordrecht, Neth.: Springer

Mackenzie FT, Lerman A, Andersson AJ. 2004. Past and present of sediment and carbon biogeochemical cycling models. *Biogeosciences* 1:11–32

Mackenzie FT, Lerman A, Ver LMB. 1998. Role of the continental margin in the global carbon balance during the past three centuries. *Geology* 26:423–26

Mackenzie FT, Ver LM, Lerman A. 2000. Coastal-zone biogeochemical dynamics under global warming. *Int. Geol. Rev.* 42:193–206

Mackenzie FT, Ver LM, Lerman A. 2002. Century-scale nitrogen and phosphorus controls of the carbon cycle. *Chem. Geol.* 190:13–32

Martínez ML, Intralawan A, Vázquez G, Pérez-Maqueo O, Sutton P, Landgrave R. 2007. The coasts of our world: ecological, economic and social importance. *Ecol. Econ.* 63:254–72

Mathis JT, Osborne E, Starkweather S. 2017. Collecting environmental intelligence in the new Arctic. In *Arctic Report Card 2017*, ed. J Richter-Menge, JE Overland, JT Mathis, E Osborne, pp. 85–91. Washington, DC: NOAA

Mathis M, Elizalde A, Mikolajewicz U. 2019. The future regime of Atlantic nutrient supply to the Northwest European Shelf. *J. Mar. Syst.* 189:98–115

Mayer B, Rixen T, Pohlmann T. 2018. The spatial and temporal variability of air-sea CO_2 fluxes and the effect of net coral reef calcification in the Indonesian Seas: a numerical sensitivity study. *Front. Mar. Sci.* 5:116

Mayorga E, Seitzinger SP, Harrison JA, Dumont E, Beusen AHW, et al. 2010. Global Nutrient Export from WaterSheds 2 (NEWS 2): model development and implementation. *Environ. Model. Softw.* 25:837–53

Meier HEM, Edman M, Eilola K, Placke M, Neumann T, et al. 2019. Assessment of uncertainties in scenario simulations of biogeochemical cycles in the Baltic Sea. *Front. Mar. Sci.* 6:46

Meier HEM, Edman MK, Eilola KJ, Placke M, Neumann T, et al. 2018. Assessment of eutrophication abatement scenarios for the Baltic Sea by multi-model ensemble simulations. *Front. Mar. Sci.* 5:440

Miura T, Suga T, Hanawa K. 2002. Winter mixed layer and formation of dichothermal water in the Bering Sea. *J. Oceanogr.* 58(6):815–23

Mizobata K, Saitoh SI, Shiomoto A, Miyamura T, Shiga N, et al. 2002. Bering Sea cyclonic and anticyclonic eddies observed during summer 2000 and 2001. *Prog. Oceanogr.* 55:65–75

Müller JD, Schneider B, Rehder G. 2016. Long-term alkalinity trends in the Baltic Sea and their implications for CO_2-induced acidification. *Limnol. Oceanogr.* 61:1984–2002

O'Mara NA, Dunne JP. 2019. Hot spots of carbon and alkalinity cycling in the coastal oceans. *Sci. Rep.* 9:4434

Pendleton L, Donato DC, Murray BC, Crooks S, Jenkins WA, et al. 2012. Estimating global "blue carbon" emissions from conversion and degradation of vegetated coastal ecosystems. *PLOS ONE* 7:e43542

Pörtner H-O, Roberts DC, Masson-Delmotte V, Zhai P, Tignor M, et al., eds. 2019. *The IPCC Special Report on the Ocean and Cryosphere in a Changing Climate.* Geneva: IPCC

Previdi M, Fennel K, Wilkin J, Haidvogel D. 2009. Interannual variability in atmospheric CO_2 uptake on the northeast U.S. continental shelf. *J. Geophys. Res.* 114(G4):G04003

Regnier P, Arndt S, Goossens N, Volta C, Laruelle GG, et al. 2013a. Modelling estuarine biogeochemical dynamics: from the local to the global scale. *Aquat. Geochem.* 19:591–626

Regnier P, Friedlingstein P, Ciais P, Mackenzie FT, Gruber N, et al. 2013b. Anthropogenic perturbation of the carbon fluxes from land to ocean. *Nat. Geosci.* 6:597–607

Ribbat B, Roether W, Münnich KO. 1976. Turnover of Eastern Caribbean deep water from ^{14}C measurements. *Earth Planet. Sci. Lett.* 32:331–41

Roeske T, Bauch D, Loeff MRVD, Rabe B. 2012. Utility of dissolved barium in distinguishing North American from Eurasian runoff in the Arctic Ocean. *Mar. Chem.* 132–133:1–14

Roobaert A, Laruelle GG, Landschützer P, Gruber N, Chou L, Regnier P. 2019. The spatiotemporal dynamics of the sources and sinks of CO_2 in the global coastal ocean. *Glob. Biogeochem. Cycles* 33:1693–714

Sarmiento JL, Gruber N. 2002. Sinks for anthropogenic carbon. *Phys. Today* 55:30

Schauer U, Fahrbach E, Osterhus S, Rohardt G. 2004. Arctic warming through the Fram Strait: oceanic heat transport from 3 years of measurements. *J. Geophys. Res.* 109(C6):C06026

Schiller RV, Kourafalou VH. 2014. Loop current impact on the transport of Mississippi River waters. *J. Coast. Res.* 30:1287–306

Schneider B, Gustafsson E, Sadkowiak B. 2014. Control of the mid-summer net community production and nitrogen fixation in the central Baltic Sea: an approach based on pCO2 measurements on a cargo ship. *J. Mar. Syst.* 136:1–9

Schneider B, Müller JD. 2018. *Biogeochemical Transformations in the Baltic Sea—Observations Through Carbon Dioxide Glasses*. Cham, Switz.: Springer

Sheu DD, Chou WC, Wei CL, Hou WP, Wong G, Hsu CW. 2010. Influence of El Niño on the sea-to-air CO_2 flux at the SEATS time-series site, northern South China Sea. *J. Geophys. Res.* 115(C10):C10021

Siedlecki SA, Pilcher D, Howard EM, Deutsch C, MacCready P, et al. 2021. Coastal processes modify projections of some climate-driven stressors in the California Current System. *Biogeosciences* 18:2871–90

Signorini SR, Mannino A, Najjar RG Jr., Friedrichs MAM, Cai W-J, et al. 2013. Surface ocean pCO_2 seasonality and sea-air CO_2 flux estimates for the North American east coast. *J. Geophys. Res. Oceans* 118:5439–60

Smith SV, Hollibaugh JT. 1993. Coastal metabolism and the oceanic organic-carbon balance. *Rev. Geophys.* 31:75–89

Smith SV, Mackenzie FT. 2016. The role of $CaCO_3$ reactions in the contemporary oceanic CO_2 cycle. *Aquat. Geochem.* 22:153–75

St-Laurent P, Friedrichs MAM, Najjar RG, Shadwick EH, Tian H, Yao Y. 2020. Relative impacts of global changes and regional watershed changes on the inorganic carbon balance of the Chesapeake Bay. *Biogeosciences* 17:3779–96

Sun H, Gao Z, Qi D, Chen B, Chen L, Cai W-J. 2020. Surface seawater partial pressure of CO_2 variability and air-sea CO_2 fluxes in the Bering Sea in July 2010. *Cont. Shelf Res.* 193:104031

Sydeman WJ, Garcia-Reyes M, Schoeman DS, Rykaczewski RR, Thompson SA, et al. 2014. Climate change and wind intensification in coastal upwelling ecosystems. *Science* 345:77–80

Takeshita Y, Frieder CA, Martz TR, Ballard JR, Feely RA, et al. 2015. Including high-frequency variability in coastal ocean acidification projections. *Biogeosciences* 12:5853–70

Terhaar J, Lauerwald R, Regnier P, Gruber N, Bopp L. 2021. Around one third of current Arctic Ocean primary production sustained by rivers and coastal erosion. *Nat. Commun.* 12:169

Thomas H, Bozec Y, Elkalay K, de Baar HJW. 2004. Enhanced open ocean storage of CO_2 from shelf sea pumping. *Science* 304:1005

Tjiputra JF, Schwinger J, Bentsen M, Moree AL, Gao S, et al. 2020. Ocean biogeochemistry in the Norwegian Earth System Model version 2 (NorESM2). *Geosci. Model Dev.* 13:2393–431

Tsunogai S, Watanabe S, Sato T. 1999. Is there a "continental shelf pump" for the absorption of atmospheric CO_2? *Tellus B Chem. Phys. Meteorol.* 51:701–12

Turi G, Lachkar Z, Gruber N. 2014. Spatiotemporal variability and drivers of pCO_2 and air–sea CO_2 fluxes in the California Current System: an eddy-resolving modeling study. *Biogeosciences* 11:671–90

Valsala V, Murtugudde R. 2015. Mesoscale and intraseasonal air–sea CO_2 exchanges in the western Arabian Sea during boreal summer. *Deep-Sea Res. I* 103:101–13

Wang GZ, Shen SSP, Chen Y, Bai Y, Qin H, et al. 2021. Feasibility of reconstructing the summer basin-scale sea surface partial pressure of carbon dioxide from sparse in situ observations over the South China Sea. *Earth Syst. Sci. Data* 13:1403–17

Wanninkhof R. 2014. Relationship between wind speed and gas exchange over the ocean revisited. *Limnol. Oceanogr. Methods* 12:351–62

Wanninkhof R, Park GH, Takahashi T, Sweeney C, Feely R, et al. 2013. Global ocean carbon uptake: magnitude, variability and trends. *Biogeosciences* 10:1983–2000

Ward BA, Friedrichs MAM, Anderson TR, Oschlies A. 2010. Parameter optimisation techniques and the problem of underdetermination in marine biogeochemical models. *J. Mar. Syst.* 81:34–43

Wollast R. 1991. The coastal organic carbon cycle; fluxes, sources, and sinks. *Ocean Margin Process. Glob. Change* 1991:365–81

Wollast R. 1993. Interactions of carbon and nitrogen cycles in the coastal zone. In *Interactions of C, N, P and S Biogeochemical Cycles and Global Change*, ed. R Wollast, FT Mackenzie, L Chou, pp. 195–210. Berlin: Springer

Wu C-R, Wang Y-L, Lin Y-F, Chao S-Y. 2017. Intrusion of the Kuroshio into the South and East China Seas. *Sci. Rep.* 7:7895

Xiao Y, Friedrichs MAM. 2014. Using biogeochemical data assimilation to assess the relative skill of multiple ecosystem models in the Mid-Atlantic Bight: effects of increasing the complexity of the planktonic food web. *Biogeosciences* 11:3015–30

Xiu P, Chai F, Curchitser EN, Castruccio FS. 2018. Future changes in coastal upwelling ecosystems with global warming: the case of the California Current System. *Sci. Rep.* 8:2866

Xu Y-Y, Cai W-J, Wanninkhof R, Salisbury J, Reimer J, Chen B. 2020. Long-term changes of carbonate chemistry variables along the North American East Coast. *J. Geophys. Res. Oceans* 125:e2019JC015982

Yang W, Guo X, Cao Z, Xu Y, Wang L, et al. 2021. Seasonal dynamics of the carbonate system under complex circulation schemes on a large continental shelf: the northern South China Sea. *Prog. Oceanogr.* 197:102630

Yu LQ, Gan JP, Dai MH, Hui CR, Lu ZM, Li D. 2021. Modeling the role of riverine organic matter in hypoxia formation within the coastal transition zone off the Pearl River Estuary. *Limnol. Oceanogr.* 66:452–68

Yuan DL, Hao JJ, Li JL, He L. 2018. Cross-shelf carbon transport under different greenhouse gas emission scenarios in the East China Sea during winter. *Sci. China Earth Sci.* 61:659–67

Zhang J, Guo X, Zhao L. 2019. Tracing external sources of nutrients in the East China Sea and evaluating their contributions to primary production. *Prog. Oceanogr.* 176:102122

Zhang S, Rutgersson A, Philipson P, Wallin MB. 2021. Remote sensing supported sea surface pCO2 estimation and variable analysis in the Baltic Sea. *Remote Sens.* 13:259

Zhao H, Dai M, Gan J, Zhao X, Lu Z, et al. 2021. River-dominated pCO_2 dynamics in the northern South China Sea during summer: a modeling study. *Prog. Oceanogr.* 190:102457